PHYSICAL REVIEW B **82**, 214515 (2010)

Renormalization group flow, competing phases, and the structure of superconducting gap in multiband models of iron-based superconductors

Saurabh Maiti and Andrey V. Chubukov
Department of Physics, University of Wisconsin, Madison, Wisconsin 53706, USA
(Received 5 October 2010; revised manuscript received 18 November 2010; published 20 December 2010)

We perform an analytical renormalization group (RG) study to address the role of Coulomb repulsion, the competition between extended s-wave superconducting order ($s\pm$), and the spin-density wave (SDW) order and the angular dependence of the superconducting gap in multipocket models of iron-based superconductors. Previous analytic RG studies considered a toy model of one hole and one electron pocket. We consider more realistic models of two electron pockets and either two or three hole pockets, and also incorporate angular dependence of the interactions. In a toy two-pocket model, SDW order always wins over $s\pm$ order at perfect nesting; $s\pm$ order only appears when doping is finite and RG flow extends long enough to overcome intrapocket Coulomb repulsion. For multipocket models, there are two new effects. First, in most cases there exists an attractive component of the interaction in $s\pm$ channel no matter how strong intrapocket repulsion is, such that the system necessary becomes a superconductor once it overcomes the competition from the SDW state. Second, in four-pocket case (but not in five-pocket case), $s\pm$ order wins over SDW order even for perfect nesting, if RG flow extends long enough, suggesting that SDW order is not a necessary precondition for the $s\pm$ order. Our analytic results are in full agreement with recent numerical functional RG studies by Thomale *et al.* [arXiv:1002.3599 (unpublished)]

DOI: 10.1103/PhysRevB.82.214515 PACS number(s): 74.20.Rp, 74.25.Dw, 74.62.Dh

I. INTRODUCTION

Since 2008 a lot of efforts in condensed-matter community have been devoted to solve the puzzle of high-T_c superconductivity (SC) in recently discovered Fe-based superconductors. To a large extent, in two years the community managed to obtain the data for the pnictides in the amount comparable to that collected for the cuprates over 20 years.[1]

The family of Fe-based superconductors is already large and keeps growing. It includes doped 1111 systems RFeAsO (R=rare-earth element),[2–5] doped 122 systems XFe$_2$As$_2$ (X=alkaline-earth metals),[6–8] as well as 111 and 11 systems like LiFeAs (Ref. 9) and FeTe/Se.[10] The parent compounds of most of these materials exhibit a spin-density wave (SDW) order,[11] and superconductivity emerges upon either hole or electron doping, or upon gradual substitution of one pnictide by the other (As by P). In some systems, like LiFeAs (Ref. 9) and LaFePO,[12] SC was found already without doping, instead of a magnetically ordered state.

ARPES,[13] de Haas–van Alphen oscillations measurements,[14] and first-principles calculations[15–17] all show that low-energy electronic structure of pnictides in two-dimensional basal plane consists of two nearly circular, nonequivalent hole pockets located at the center of the Brillouin zone (BZ), and two symmetry-related elliptical electron pockets, located near the corners of the BZ in the folded zone scheme, or near $(0,\pi)$ and $(\pi,0)$ points, respectively, in the unfolded zone scheme. [Folded and unfolded zones differ in treating the pnictides—folded zone takes into account the fact that there are two nonequivalent positions of pnictides above and below Fe plane, and has two Fe atoms in the unit cell, while unfolded zone incorporates only Fe atoms and has one Fe atom in the unit cell.] These hole and electron pockets form warped cylinders in three-dimensional (3D) space. In addition, in some pnictides there is a fifth cylindrical hole pocket centered at (π,π) in the unfolded zone (at (0,0) in the folded zone, like other two hole pockets) while in other pnictides this fifth Fermi surface (FS) becomes a 3D sphere centered near $k_z=\pi$ along z direction.

A lot of work has been done over the last two years regarding the symmetry of the order parameter and the interplay between SDW and SC orders. Most of researchers (but not all, see Ref. 18) believe that the gap symmetry is extended s-wave ($s\pm$), meaning the gap transforms according to A_{1g} representation of D_{4h} tetragonal symmetry group, but the average gap values along hole and electron Fermi surfaces have different sign. However, the structure of the gap is still a puzzle. Early works based on either spin-fluctuation scenario[17,19–21] or on renormalization group (RG) study of a toy model of one hole and one electron FS (Refs. 22 and 23) found a simple angle-independent $s\pm$ gap. Subsequent more sophisticated numerical studies, which take into account multiorbital nature of low-energy excitations in the pnictides, have reported angular dependence of the $s\pm$ gap, with $\cos 2\phi$ variations on the electron FSs and $\cos 4\phi$ variations along the hole FSs.[20,24–27] The $\cos 2\phi$ modulations of the $s\pm$ gap on the electron FSs has also been obtained in the analytical study.[28] If $\cos 2\phi$ variation is strong enough, the gap has "accidental" nodes along electron FSs, still preserving $s\pm$ symmetry.

Other recent theory proposals include s^{++} state,[18] $s\pm$ state with nodes on hole FSs due to strong $\cos 4\phi$ modulations,[29] and s^{+-} state with nodes at particular k_z along z direction.[3]

Experiments are generally consistent with $s\pm$ gap symmetry but whether or not the gap has nodes, in particular, materials is still subject of debate.[30–42] In addition, there is no information yet from the experiments where the gap nodes are located, if present. ARPES measurements of the gap along hole FSs (taken at fixed k_z) on various Fe pnictides[43–45] indicate that the gap is almost angle indepen-

dent but the detailed measurements of the gap separately along each of the two electron FSs are still lacking, with only few exceptions.[46]

From theoretical perspective, the most relevant issue is the nature of the pairing interaction. Conventional electron-phonon coupling is always a candidate, particularly when the gap has *s*-wave symmetry, but has been shown to be rather weak,[16] and is incapable to account for $T_c \sim 50$ K even if one neglects destructive effect of Coulomb interaction. This leaves electron-electron interaction (i.e., dressed Coulomb repulsion at a finite momentum transfer) as the dominant pairing interaction. Such interaction cannot give rise to a constant *s*-wave gap, but it can give rise to either momentum-dependent, sign reversing gap along a given FS, like $d_{x^2-y^2}$ gap in the cuprates, or to gaps of different signs along different FSs. Coulomb interaction at large momentum transfer contributes to the pairing both directly and by creating effective pairing interactions mediated by collective excitations in either spin or charge channel. The close proximity to magnetism makes spin fluctuations a preferable candidate,[17,19,24] although orbital fluctuations were also considered recently.[47] Both direct Coulomb interaction (the pair hopping) and magnetically mediated interaction are attractive for $s\pm$ gap, and the total attractive pairing interaction is a combination of the two. Still, to give rise to a pairing, this combined attractive pairing interaction has to overcome repulsion coming from Coulomb interaction at small momentum transfers. A conventional McMillan-Tolmachev renormalization[48] does not help here because both repulsive and attractive parts of the interaction renormalize in the same way, and if repulsive part is initially stronger, the renormalization just reduces the strength of the total repulsive interaction, but cannot change its sign.

How to overcome Coulomb interaction became the major issue for *s*-wave pairing in the pnictides. The situation is further complicated by the fact that low-energy excitations are composed of all five hybridized Fe 3*d* orbitals, and Coulomb interactions between fermions belonging to a given orbital and belonging to different orbitals are equally important. Only if all of these interactions are approximated by the same momentum-independent Hubbard *U*, this *U* cancels out in the pairing problem and one is left with a pure spin-mediated interaction (this was termed "Coulomb avoidance"[49]). In reality, Coulomb interaction is momentum dependent and is larger at a small momentum transfer than at a large momentum transfer, and intraorbital and interorbital interactions are also different. As a result, direct Coulomb pairing interaction is repulsive for superconductivity with angle-independent plus-minus gap. Spin-mediated interaction is attractive and can potentially compete with direct Coulomb repulsion. However, at least at weak/moderate coupling direct Coulomb repulsion is the largest term. This holds even when magnetic correlation length ξ diverges because for the pairing one generally needs the interaction at nonzero frequencies, where it remains finite.

There are two possibilities to obtain $s\pm$ superconductivity despite strong Coulomb repulsion. First, multiorbital character of excitations in the pnictides implies that the attractive pairing interaction (either pair hopping or spin-fluctuation exchange) is angle dependent. The angle dependence comes from coherent factors which dress up the interactions when one transforms from the orbital picture—in which different parts of the Fermi surface are made of different orbitals—to the band picture, in which free-fermion part is simply $\epsilon_k c_k^\dagger c_k$, and all information about multiorbital character is passed onto interactions. Once interaction is angle dependent, the gap also becomes angle dependent, and the system adjusts the angle dependence of the gap to minimize the effect of Coulomb repulsion (we discuss this in more detail below). The most natural is the case when the gap acquires $\pm\cos 2\phi$ components along the two electron FSs, and the magnitude of this component is adjusted to balance the interplay between small q Coulomb repulsion and the combined attractive interaction in $s\pm$ channel. When Coulomb repulsion dominates, the angle-dependent part is large, and the gap has four nodes along each of the electron FSs.

Second, one can analyze how the interactions evolve as the system flows toward smaller energies, relevant to superconductivity. This flow involves renormalizations of interactions in both particle-hole (p-h) and particle-particle (p-p) channel, and goes beyond random-phase approximation (RPA). This flow has been studied numerically, using functional RG (fRG) technique[25–27] and analytically,[22,28,50] within parquet RG. Both are weak-coupling studies, based on the Hamiltonian which contains screened Coulomb interaction, but no additional spin-fluctuation interaction. The results of both types of studies are quite similar: it turns out that Coulomb repulsion at small momentum transfers decreases upon system flow to smaller energies but the pairing interaction at large momentum transfers (the pair hopping from hole to electron FSs), which is attractive for $s\pm$ superconductivity increases. The increase in the pair hopping is the result of the "push" from the interpocket density-density interaction which by itself leads to SDW instability. If RG flow of the couplings persists over a wide enough range of energies, pair-hopping interaction exceeds Coulomb repulsion, and the system develops an attraction in the $s\pm$ channel. In this situation, the $\pm\cos 2\phi$ variations in the gap on electron FSs induced by angle dependence of the interaction, are not crucial for the pairing, and the system can develop an $s\pm$ gap without nodes.

While this scenario is quite generic, the earlier parquet RG study[22,50] was more limited in scope. It was done for a toy model of one hole and one electron FS centered at (0,0) and (π,π), respectively. For such a model, angle dependencies of the interactions must be symmetric with respect to interchanging x and y momentum components both near $k=(0,0)$ and $k=(\pi,\pi)$ and can only be in the form $\cos 4\phi$, $\cos 8\phi$, etc., which are subleading terms in the expansion of A_{1g} gap for a single FS (no $\cos 2\phi$ terms). Such $\cos 4n\phi$ terms are generally irrelevant and were neglected in toy model analysis, i.e., the gap along each of the FSs was approximated by a constant. Like we said, for momentum-independent gaps, the bare interaction in the $s\pm$ channel is repulsive if intrapocket Coulomb repulsion is the largest. The interaction flows under RG and changes sign at some value of RG parameter. Still, all along parquet RG flow, the pairing interaction remains secondary to the interaction in the SDW channel. As a result, for perfect nesting the system develops an SDW order. Only when the system is doped and the loga-

rithmical flow of the SDW vertex is cut at low energies, SC channel takes over and the system develops a $s\pm$ superconductivity.

In the present paper we extend earlier parquet RG analysis to multipocket models of Fe pnictides. We consider two models. The first one has two electron FSs, located at $(0,\pi)$ and $(\pi,0)$ in the unfolded zone, and two hole FSs located near (0,0). The second model has an additional hole pocket centered at (π,π) in the folded zone. The presence or absence of this additional FS in different Fe pnictides is attributed[19,27] to the difference in the distance between the pnictide (e.g., As or P) and the Fe plane. To avoid overly complicated analysis of RG equations we only consider two limiting cases: one when the two hole pockets centered at (0,0) are completely equivalent, and the other when one pocket is coupled to electron FSs much weaker than the other one and can be neglected (this effectively reduces four-pocket model to three pockets and five-pocket model to four pockets). The system behavior is identical in the two limits which gives us confidence that it remains the same also in between the limits. Throughout the paper we assume that all FSs are cylindrical and neglect their variations along k_z.

We argue that new features: nodal $s\pm$ SC and appearance of SC even at perfect nesting, emerge once one extends the model from two to four pocket (or to three pocket when only one hole FS is relevant). This result is consistent with early assertions[22,28] that the three-pocket model is the minimum model needed to understand the key physics of Fe pnictides. The behavior of five-pocket model, on the contrary, is in many respects similar to that for two-pocket model (except that nodal $s\pm$ SC is still possible). That four-pocket and five-pocket models behave differently under RG has been the conclusion of fRG study by Thomale *et al.* (Ref. 27), and our results fully agree with their analysis.

We extend previous two-pocket study in two directions. First, we incorporate $\cos 2\phi$ angular dependence of the interactions which give rise to $\pm\cos 2\phi$ modulations of the gaps on electron FSs. In this situation, there are at least three different effective vertices for $s\pm$ gap symmetry, and we argue that, if the dominant angle dependence comes from electron-hole interaction, one of them remains positive (i.e., attractive) over the entire RG flow even when bare intrapocket repulsion is the largest interaction. We show that the stronger is the angular dependence of the interaction, the stronger is the tendency to develop a nodal $s\pm$ order.

Second, we reanalyze the interplay between SC and SDW channels. For angular-dependent interactions, are also several SDW vertices of which at least one is attractive along the whole RG trajectory. We compare the flow of the leading vertices in SDW and SC channel. We show that in four-pocket model, the trajectory of the leading SC vertex are steeper than that of the leading SDW vertex, and the latter remains larger only down to some RG scale. At smaller scales (i.e., when RG flow extends further to lower energies) the SC vertex overshadows SDW vertex even at perfect nesting. This agrees with fRG study by Thomale *et al.*[27] We argue, based on our analytic consideration, that the crossing between SC and SDW vertices under RG flow is to a large extent a combinatoric effect—compared to two-pocket case (where SDW and SC vertices flow to the same value under RG), the presence of the two electron FSs adds the factor of 2 to the renormalization of the SC vertex as the pair hopping can, e.g., hop a pair of $k,-k$ fermions from the hole FS to each of the two electron FSs but momentum conservation does not allow such factor of 2 to appear in the renormalization of the SDW vertex.

We further find that for five-pocket model, SC vertex always remains secondary compared to SDW vertex, just like in two-pocket model. Furthermore, like in two-pocket model, SC and SDW vertices flow to the same value at the fixed point. This again agrees with fRG result by Thomale *et al.*

The rest of the paper is organized as follows: Sec. II outlines our approach, explains the subtleties in the RG flow, and discusses the technique by which we incorporate the momentum dependence into our analysis. In Sec. III we briefly review the results for the two-pocket case. Section IV is the central section in the paper—here we consider in detail the four-pocket model. We discuss SC vertices in the presence of angular dependence of the interaction, the RG flow, and the competition between SC and SDW instabilities. Most of our treatment in this section is for the limit when one of the hole FS can be neglected. Later in the section we analyze another limit when the two hole FS are equivalent and show that the system behavior is identical in the two limits. In Sec. V we discuss five-pocket model and argue that its behavior to a large extent is similar to that in two-pocket model. We summarize our results in Sec. VI.

II. DISCUSSIONS

Before starting the detailed description of each model, we present a brief discussion on the outline of our approach. We first describe the central idea behind our analysis, then describe the technique through which we incorporate the angular dependence of the vertices and finally discuss how we incorporate these into RG equations.

A. Approach

We consider four-fermion interactions between fermions located close to the FSs of two or more pockets. We consider Hamiltonian with all possible quartic interactions allowed by symmetry and ask what can be said about the onset of SC, SDW, and, possibly, charge-density-wave (CDW) instabilities. The usual approach is to write down equations for effective vertices Γ_i in SDW, SC, CDW channels and check for the existence of critical temperatures $T_{ins}^{(i)}$ at which Γ_i diverges. In case of competing instabilities, the equations for the effective vertices are coupled and, once the coupled system is solved, the instability with the highest $T_{ins}(T_c)$ takes over.

As we said in Sec. I, when one does such an analysis, one deals with interactions taken at the scale of T_c, which are not the same as the terms in the Hamiltonian. To account for the flow of the couplings from the scale of the bandwidth down to T_c, we need RG analysis. This analysis assumes renormalizability of the theory and can be rigorously justified only when the RG flow is logarithmical (i.e., interactions vary as functions of the logarithm of the running scale E). One well-

known example of logarithmical RG flow is the renormalization in the particle-particle channel (Cooper renormalization). Another, specific to our case, is the renormalization in the particle-hole channel, involving intermediate fermions from hole and electron pockets. Because hole and electron dispersions are of opposite sign, such a renormalization also generates logarithmical dependence of the running energy and/or momentum as long as the running energy exceeds the sum of energies of the top of the hole band and the bottom of the electron band (hole and electron masses do not have to be equal).

The logarithmical renormalizations in the particle-particle and particle-hole channels are characterized by corresponding polarization bubbles. Let c describe a hole band centered at $k=0$ and f describe an electron band centered at Q. Assume for simplicity that hole and electron masses are equal. For a perfect nesting, hole and electron dispersions obey $\varepsilon_c(k)=\epsilon_0-k^2/(2m_h)=-\varepsilon_f(k+Q)$. The two logarithmically singular polarization bubbles are

$$\Pi_{pp}^{cc}(q,\Omega)=\Pi_{pp}^{ff}(q,\Omega)=\int \frac{d^2k\ d\omega}{(2\pi)^3}G^c(k,\omega)G^c(q-k,\Omega-\omega)$$

$$=\frac{m}{2\pi}L+\cdots,$$

$$\Pi_{ph}^{cf}(q+Q,\Omega)=\int \frac{d^2k\ d\omega}{(2\pi)^3}G^c(k,\omega)G^f(q+Q+k,\Omega+\omega)$$

$$=-\frac{m}{2\pi}L+\cdots,$$

$$L=\frac{1}{2}\ln\left(\frac{\Lambda}{E}\right) \tag{1}$$

where the dots stand for nonlogarithmic terms, $E=\max\{\Omega,v_Fq\}$ and $E>E_F$, Λ is the upper cutoff of order bandwidth, and the propagators are given by $G^x=\frac{1}{i\omega-\epsilon_k^x}$, x being c or f.

The RG study requires caution as the couplings flow differently for energy scales above E_F and below E_F. The reasoning is simple: logarithmical RG analysis requires that internal momenta in each diagram for vertex renormalization be larger than external momenta, which are of order k_F. When typical internal energies are larger than E_F, internal momenta are larger than k_F, and vertex corrections in both particle-particle and particle-hole channel are logarithmic. This gives rise to parquet RG. When typical energies are smaller than E_F, the strength of the renormalization in the particular channel depends on the interplay between external momenta. When total incoming momenta is zero, renormalization in the particle-particle channel is still logarithmically singular, but in the renormalization of the particle-hole channel, the logarithm is cut by external E_F. Conversely, for the vertex with transferred momentum equal to the distance between hole and electron FSs, the renormalization in the particle-hole channel is still logarithmical, but in the renormalization in the particle-particle channel, the logarithm is now cut by external E_F. As a result, the renormalizations in the particle-particle and particle-hole channels are coupled at energies above E_F, but become decoupled at energies below E_F. At $E<E_F$ parquet RG equations are replaced by conventional ladder RG equations $d\Gamma_i/dl=\Gamma_i^2$, where $l=\log E_F/E$. Thus the flow of the couplings splits into the flow from the bandwidth down to E_F, where different vertices are all coupled, and the flow below E_F, where different vertices are decoupled (see Fig. 1). This reasoning is particularly important in our case, as in pnictides $E_F\sim 100$ meV is much smaller than the bandwidth, which is a few electron volts.

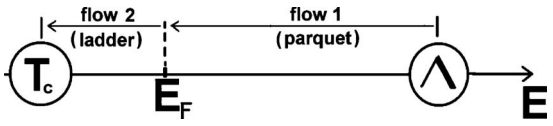

FIG. 1. Illustration showing how the couplings evolve under RG flow. The bare couplings (the parameters of the Hamiltonian) are defined at energies comparable to the bandwidth Λ. In pnictides, this scale is 2–3 eV, much larger than the Fermi energy $E_F\sim 0.1$ eV SC and SDW instabilities likely come from even smaller energies because instability temperatures are at least order of magnitude smaller than E_F. The couplings vary as one integrates out higher energies. This variation (i.e., the flow of the couplings from Λ down to the running scale E) can be generally captured by the RG technique. In pnictides, the flow is different above and below E_F. Above E_F, each of the couplings changes because of integrating out higher energy fermions in both particle-hole and particle-particle channels. The RG equations in this region are called parquet RG because renormalizations extend in the two directions. Below E_F, each vertex continue to flow due to renormalizations in only one channel, either particle-hole or particle-particle, depending on the external momenta. The RG equations in this region is called ladder RG because renormalizations extend only in one direction.

Depending on the character of the flow, the bare values of the couplings, and the ratio of the bandwidth and the Fermi energy, several situations are possible and shown in Fig. 2: (1) the RG flow diverges and the normal state becomes unstable before the scale of E_F is reached [Fig. 2(a)]. In this situation, the instability is reached already within parquet RG. This situation is the most interesting one from physics perspective particularly because in several cases different vertices diverge simultaneously, and the fixed point has an enhanced symmetry [e.g., in the two-band model, the vertices in SDW, SC, and orbital CDW channels all diverge at the fixed point which then has $O(6)$ symmetry[50,51]]. The instability at energies above E_F is, however, unlikely scenario for the pnictides because the largest instability temperature is only a fraction of E_F. (2) The RG flow reaches E_F before couplings diverge [Fig. 2(b)]. In this situation, parquet RG creates a hierarchy of the couplings at E_F: $\Gamma_i(E_F)$. Below E_F, different Γ_i decouple and, for a perfect nesting, each continue evolving according to a ladder RG, i.e., like $\Gamma_i(E)=\Gamma_i(E_F)/[1-\Gamma_i(E_F)\log\frac{E_F}{E}]$. The instability occurs at the energy (temperature) at which $\Gamma_i(E_F)\log\frac{E_F}{E}=1$. Obviously, the winning channel is the one in which the coupling is the largest at E_F. (3) When nesting is not perfect (i.e., energies of the top of the hole band and of the bottom of the electron band are not exactly opposite), the coupling in the SC channel continues to follow $\Gamma^{SC}(E)=\Gamma^{SC}(E_F)/[1-\Gamma^{SC}(E_F)\log\frac{E_F}{E}]$

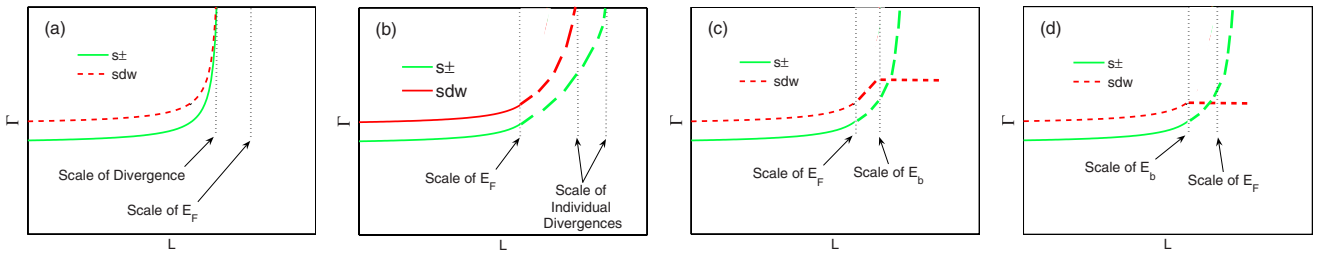

FIG. 2. (Color online) Schematics of the RG flow of SC and SDW vertices Γ^{SDW} and $\Gamma^{s\pm}$. The horizontal scale is $L=\frac{1}{2}\ln\frac{\Lambda}{E}$ for $E>E_F$ and $\frac{1}{2}\ln\frac{\Lambda}{E_F}+\ln\frac{E_F}{E}$ for $E<E_F$. SC and SDW vertices remain coupled at energies larger than E_F but decouple below E_F. Depending on the bare values of the vertices, the ratio Λ/E_F, and the doping, four different scenarios are possible (panels (a)-(d)). For perfect nesting, there are two possibilities: (a) the vertices diverge at the same scale before the scale of E_F is reached. The ratio of the vertices not necessarily tends to one, though. (b) E_F is reached before the vertices diverge. Then, below E_F, the vertices decouple, flow, and diverge independently, each on its own scale. The vertex that had larger value at E_F diverges first and sets the instability. For non-perfect nesting (e.g., at a finite doping), SDW vertex eventually does not diverge. SC vertex still diverges, and the system becomes a SC even if SC instability was subleading at perfect nesting. The flow of the SDW vertex levels off either at $E_b<E_F$ [panel (c)], or at $E_b>E_F$ [panel (d)].

simply because SC instability involves pairs of fermions with $\mathbf{k}$ and $-\mathbf{k}$ from the same FS and is nonsensitive to a deviation from perfect nesting. However the logarithmic flow of SDW and CDW vertices is now cut at some scale E_b. Suppose $E_b<E_F$ [Fig. 2(c)]. In this situation, SC eventually wins over SDW and CDW instabilities, even if superconducting Γ is subleading at E_F (but it needs to be attractive at E_F). (4) When E_b exceeds E_F [Fig. 2(d)] particle-hole and particle-particle channels decouple already within the applicability range of parquet RG. At $E<E_b$, SC vertex continue to grow as $\Gamma^{\mathrm{SC}}(E)=\Gamma^{\mathrm{SC}}(E_b)/[1-\Gamma^{\mathrm{SC}}(E_b)\log E_b/E]$ while vertices in density-wave channels get frozen at their values at $E\sim E_b$. In this situation, SC instability again wins, even if it was subleading at E_b, provided that the superconducting vertex is attractive at E_b.

A subtle point: below we will be presenting the RG flows of vertices and couplings at energies both above and below E_F in terms of the logarithmic variable $L\sim\log E$. One has to bear in mind, however, that the prefactor for the logarithm actually changes between $E>E_F$ and $E<E_F$ because for $E>E_F$ the integration over intermediate energies involves only positive excitations for electron states (and negative for hole state), i.e., $\int\frac{d^2k}{(2\pi)^2}=(m/2\pi)\int_E^\Lambda d\epsilon_k$ while for $E<E_F$, one has to linearize the dispersions of holes and electrons near the FS and integrate on both sides of E_F, i.e., $\int\frac{d^2k}{(2\pi)^2}=(m/\pi)\int_E^{E_F}d\epsilon_k$. To simplify the presentation we just define

$$L=\begin{cases}\frac{1}{2}\ln\frac{\Lambda}{E}, & E>E_F\\ \frac{1}{2}\ln\frac{\Lambda}{E_F}+\ln\frac{E_F}{E}, & E<E_F\end{cases}$$

and use the same symbol L for all energies. This is valid as long as we describe the system behavior at $E\gg E_F$ and $E\ll E_F$. The behavior in the crossover regime $E\sim E_F$ is more complex but this is beyond the scope of the present paper. We will also use $L_{E_F}\equiv\frac{1}{2}\ln\frac{\Lambda}{E_F}$.

B. Incorporating angular dependence

As we said in Sec. I, multiorbital character of low-energy excitations in Fe pnictides implies that interactions between fermions located near hole or electron FSs depend on the angles along the FSs. To obtain angular dependence of various couplings from first principles, one has to transform from five-orbital to five-band picture and dress up Coulomb interactions by coherence factors. This has been done in several studies (see, e.g., Refs. 24, 26, and 52), under the assumption that the Coulomb interaction is so strongly screened that it can be replaced by Hubbard U. This assumption is generally valid for systems with large FSs, because of many available particle-hole pairs for screening, but in systems with small FSs, like pnictides, much fewer number of particle-hole pairs are available, and the screening of Coulomb interaction is much weaker, and is actually a rather nontrivial phenomenon at small k_F (Ref. 53) Because of this complication, the "first-principles" analysis of the angular dependence of the interaction is a rather difficult task.

One can, however, attempt to extract these angular dependence from symmetry considerations, like it has been done for the cuprates[54] This is what we will do. Consider first the pairing vertex between fermions with incoming momenta k and $-k$ and outgoing momenta p and $-p$. Quite generally, for tetragonal D_{4h} symmetry group, this interaction can be divided into one- and two-dimensional representation, and one-dimensional representation can be further divided into A_{1g}, B_{1g}, B_{2g}, and A_{2g} harmonics, depending on the symmetry under the transformations under $k_{x,y}\to-k_{x,y}$ and $k_x\to k_y$. Basic functions from different representations do not mix but each contains infinite number of components. s-wave pairing corresponds to fully symmetric A_{1g} representation. The s-wave pairing interaction can be quite generally expressed as

$$u(k,p)=\sum_{m,n}A_{mn}\Psi_m(k)\Psi_n(p), \tag{2}$$

where $\Psi_m(k)$ are the basis functions of the A_{1g} symmetry group: 1, $\cos k_x\cos k_y$, $\cos k_x+\cos k_y$, etc., and A_{mn} are coefficients. Suppose for definiteness that k belongs to hole FS and is close to $k=0$. Expanding *any* wave function with A_{1g} symmetry near $k=0$, one obtains along $|\mathbf{k}|=k_F$,

$$\Psi_m(k) = a_m + b_m \cos 4\phi_k + c_m \cos 8\phi_k + \cdots . \quad (3)$$

If **p** is near the same hole FS, the expansion of $\Psi_n(p)$ also involves $\cos 4\phi_p, \cos 8\phi_p$, etc. There are no fundamental reasons to expect that b_m, c_m, etc are much smaller than a_m but subleading terms are often small numerically. Two known examples are the numerical smallness of $\cos 6\phi$, etc., components of the $d_{x^2-y^2}$-wave gap for spin-fluctuation mediated pairing in the cuprates[55] and the numerical smallness of $\cos 4\phi$, etc components of the gap along the hole FSs in fRG (Ref. 27) and RPA (Refs. 24 and 56) calculations for five-band Hubbard-type model for the pnictides. Taking these examples as circumstantial evidence, we assume that $\cos 4\phi$, etc., terms are small. If so, the interaction between fermions belonging to the hole FS can be approximated by angle-independent term.

The situation changes, however, when we consider pairing interaction between fermions belonging to different FSs. Suppose that k are still near the center of the Brillouin zone, but p are near one of the electron FSs, say the one centered at $(0,\pi)$. Consider all possible $\Psi_n(p)$ with A_{1g} symmetry. A simple experimentation with trigonometry shows that there are two different subsets of basic functions

$$A{:}1, \quad \cos p_x \cos p_y, \quad \cos 2p_x + \cos 2p_y \ldots ,$$

$$\bar{A}{:}\cos p_x + \cos p_y, \quad \cos 3p_x + \cos 3p_y \ldots \quad (4)$$

Functions from class A have the same properties as before—they can be expanded in series of $\cos 4l\phi_p$ (l is integer). Functions from class $\bar{A}$ are different—they all vanish at $(0,\pi)$ and are expanded in series of $\cos(2\phi_p + 4l\phi_p)$ (i.e., the first term is $\cos 2\phi_p$, the second is $\cos 6\phi_p$, etc.). Let's make the same approximation as before and neglect all terms with $l > 0$. The functions from class A can then be approximated by a constant, but the functions from class $\bar{A}$ are approximated by $\cos 2\phi_p$. As a result, s-wave pairing interaction involving fermions from hole and one of the two electron FSs (labeled as e_1) has a generic form of

$$u_{e_1,h}(k,p) = u_{e_1,h} + \bar{u}_{e_1,h} \cos 2\phi_{p_{e1}} + \cdots$$

$$= u_{e_1,h}(1 + 2\alpha \cos 2\phi_{p_{e1}}) + \cdots , \quad (5)$$

where dots stand for $\cos 4\phi_k, \cos 4\phi_p, \cos 6\phi_p$, etc., terms. We emphasize that the constant term and the $\cos 2\phi_p$ term in Eq. (5) are the leading terms of the two subsets of interaction terms, each form series in $\cos 4\phi_{k,p}$. By the same reasoning, the interaction between fermions near two electron FSs centered at $(0,\pi)$ and $(\pi,0)$ is expressed as

$$u_{e_1,e_2}(k,p) \sim u_{e_1,e_2}(1 + 2\alpha'(\cos 2\phi_{k_{e1}} + \cos 2\phi_{p_{e2}}) + 4\alpha'' \cos 2\phi_{k_{e1}} \cos 2\phi_{p_{e2}} + \cdots . \quad (6)$$

Observe also that the $\cos 2\phi$ terms in Eqs. (5) and (6) change sign under the transformation $x \to y$ (like $d_{x^2-y^2}$ interaction in the cuprates), hence the prefactor for $\cos 2\phi_p$ term in Eq. (5) changes sign between the two electron FSs $[\cos 2\phi_{p_{e1}} \to -\cos 2\phi_{p_{e2}}]$.

The pairing interaction in the form of Eq. (5) has been introduced in Ref. 28. The authors of Ref. 28, however, did not include into consideration the fact that band description is obtained from multiorbital description and argued that α must generally scale as k_F^2 and should be small when k_F is small. In fact, the angular dependence produced by the coherent factors associated with the hybridization of five Fe bands are not small in k_F (Refs. 24 and 52), hence $\alpha, \alpha', \alpha''$ *do not have to be small*. Accordingly, we will keep α's as just parameters.

Once the pairing interaction has the form of Eqs. (5) and (6), the gap along hole FS is still angle independent but the gaps along the two electron FSs are in the form $\Delta_e \pm \bar{\Delta}_e \cos 2\phi$. When $\bar{\Delta}_e$ is small compared to Δ_e, the gaps on electron FSs are nearly angle-independent but when $|\bar{\Delta}_e| > |\Delta_e|$, they have nodes at accidental values of ϕ.

C. RG analysis with angle-dependent interactions

The angular dependence of the interaction is the key element of fRG approach, and this approach uses the full momentum dependence of the interactions, i.e., the full series of $\cos 4l\phi$ and $\cos(2\phi + 4l\phi)$ terms. At the same time, fRG approach assumes renormalizability [i.e., that the right-hand side (r.h.s.) of each fRG equation contains only renormalized couplings, not some combinations of bare and renormalized couplings]. In our analytical approach, we do calculations within logarithmic approximation in which case we explicitly preserve renormalizability.

We found, after explicitly evaluating the renormalizations of angle-dependent vertices, that the only way to justify RG procedure in this situation is to keep the angular dependence away from RG flow, i.e., allow u_{e_1,e_2}, $u_{e1,h}$, and $u_{e2,h}$ to flow under RG while α, α', and α'' are kept unchanged. This can be rigorously justified when α's are small and all terms of order α^2 are neglected. We will assume without proof that the results of RG analysis are valid even when $\alpha \leq 1$. There are no new physical effects at $\alpha \leq 1$ compared to $\alpha \ll 1$, so the results at $\alpha \leq 1$ should be at least qualitatively correct by continuity.

As we said in Sec. I, the main goal of our analysis is to understand whether there are qualitative differences between RG flow and the pairing in two, four, and five pocket models for Fe pnictides. The next three sections deal with the comparison of two, four, and five-pocket models.

III. TWO-POCKET MODEL

This has been studied before (Refs. 22 and 50) and we briefly review it here to set notations and for further comparisons with multipocket cases. The two-pocket model is a toy model consisting of one hole pocket in the center the folded BZ, and four electron pockets at the corners as shown in Fig. 3. To obtain parquet RG equations, we consider energies larger than E_F and E_b. At such energies deviations from perfect nesting become irrelevant, and we can set $E_F, E_b \to 0$ and take hole and electron dispersions to be just opposite in sign.

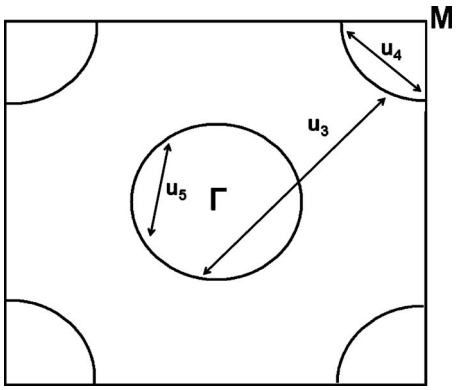

FIG. 3. Hole (center) and electron (corners) FSs in the folded BZ for two-pocket model. The arrows with symbols indicate intrapocket and interpocket pairing interactions (u_4 and u_5 are intrapocket interactions, and u_3 is interpocket interaction). There also exist density-density and exchange interactions between hole and electron pockets (u_1 and u_2 terms, respectively, not shown).

The interaction Hamiltonian for the two-pocket model is (following earlier notations[22])

$$\frac{m}{2\pi}H_{int} = \sum u_1 \; c^\dagger_{p_1 s} f^\dagger_{p_2 s'} f_{p_4 s'} c_{p_3 s} + \sum u_2 \; c^\dagger_{p_1 s} f^\dagger_{p_2 s'} c_{p_4 s'} f_{p_3 s}$$
$$+ \sum \frac{u_3}{2}(c^\dagger_{p_1 s} c^\dagger_{p_2 s'} f_{p_4 s'} f_{p_3 s} + h.c.)$$
$$+ \sum \frac{u_4}{2} f^\dagger_{p_1 s} f^\dagger_{p_2 s'} f_{p_4 s'} f_{p_3 s} + \sum \frac{u_5}{2} c^\dagger_{p_1 s} c^\dagger_{p_2 s'} c_{p_4 s'} c_{p_3 s}, \tag{7}$$

where u_i are dimensionless couplings and m is quasiparticle mass ($\varepsilon_f(k)=k^2/2m-\mu$). The sum is over the spin indices s and s' and the vector momenta p_1, p_2, p_3, p_4 with momentum conservation assumed. The c and f fermions reside at the hole and the electron bands, respectively. We remind the reader that there is no angular dependence of the interactions here because the first angular term that comes in is $\cos 4\phi$ which we ignore in our approximation.

A. Vertices

We begin by looking into the vertices in SC and SDW channels. For this, we introduce infinitesimally small SC and SDW order parameters $\Delta^o_{\rm SC}$ and $\Delta^o_{\rm SDW}$, dress them up by including multiple interactions as shown diagrammatically in Fig. 4, and write the renormalized order parameters in the form

$$\Delta_i = \Delta^o_i(1+\Gamma_i L), \tag{8}$$

where Γ_i satisfies $\frac{d\Gamma_i}{dL}=\Gamma_i^2$

For a given i, Δ_i becomes nonzero even for vanishing Δ^o_i when the corresponding Γ_i diverges. The computations for the two-pocket model is straightforward. For the SDW order parameter, we immediately obtain from Fig. 4, $\Gamma^{\rm SDW}=u_1+u_3$. For the SC channel, we obtain from Fig. 4

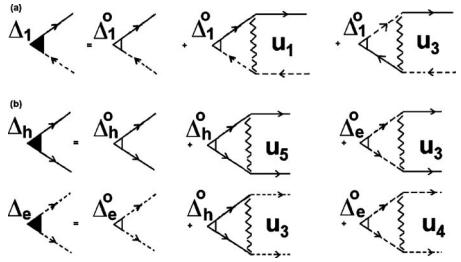

FIG. 4. Diagrams for the renormalization of infinitesimally small SDW and SC vertices, added to the Hamiltonian in order to calculate response functions. Unshaded triangles—bare vertices, shaded triangles—full vertices, wave lines—fully renormalized interactions. Solid lines correspond to c fermions and the dashed line to f fermions. Δ_1 is SDW vertex and Δ_h and Δ_e are SC vertices on hole and electron FSs.

$$\begin{pmatrix} 1-u_5 L & -u_3 L \\ -u_3 L & 1-u_4 L \end{pmatrix}\begin{pmatrix} \Delta^o_h \\ \Delta^o_e \end{pmatrix} = \begin{pmatrix} \Delta_h \\ \Delta_e \end{pmatrix}, \tag{9}$$

where $\Delta_{e,h}$ are order parameters on hole and electron FSs. Diagonalizing this set and casting the result in the form of Eq. (8), we obtain two SC Γ's. One corresponds to a conventional s-wave pairing, is repulsive for all positive u_i and is of no interest to us, another corresponds to $s\pm$ pairing and is given by

$$\Gamma^{s\pm} = \frac{-(u_4+u_5)+\sqrt{(u_4-u_5)^2+4u_3^2}}{2}. \tag{10}$$

For $u_4=u_5$, $\Gamma^{s\pm}$ reduces to $\Gamma^{s\pm}=-u_4+u_3$.

The SDW vertex is attractive for positive u_1 and u_3 while $\Gamma^{s\pm}$ is attractive only when interband pair hopping term exceeds intraband repulsive interaction. Like we said, this is very unlikely because both interactions originate from Coulomb interaction, and screened Coulomb interaction at small momentum transfer (i.e., u_4 and u_5) is larger than that at large momentum transfer (i.e., u_3). To understand whether the negative sign of $\Gamma^{s\pm}$ can be reversed, we need to consider RG flow of the couplings. This what we do next.

B. RG flow between Λ and E_F

The RG equations for the couplings have been obtained in Ref. 22, and we just quote the result

$$\dot{u}_4 = -[u_4^2+u_3^2],$$
$$\dot{u}_5 = -[u_5^2+u_3^2],$$
$$\dot{u}_1 = [u_1^2+u_3^2],$$
$$\dot{u}_2 = [2u_1u_2-2u_2^2],$$
$$\dot{u}_3 = [4u_1u_3-2u_2u_3-(u_4+u_5)u_3]. \tag{11}$$

The derivatives are with respect to L. These equations have a single nontrivial fixed point at which all couplings diverge and tend to $u_3=\sqrt{5}u_1, u_4=u_5=-u_1, u_2\propto(u_1)^{1/3}$. The flow of

SDW and SC vertices is shown in Fig. 6(a). In the process of RG flow, the SC vertex $\Gamma^{s\pm}$ changes sign and become attractive. The ratio $\Gamma^{s\pm}/\Gamma^{\mathrm{SDW}}$ remains smaller than one during the flow, but tends to one upon approaching the fixed point, i.e., if this fixed point is reached within parquet RG, superconducting and SDW instabilities occur simultaneously, and the system actually cannot distinguish between the two. There is another vertex which tends to the same value as SDW and SC vertices-it corresponds to an CDW instability with imaginary order parameter (an instability toward orbital currents), The combination of three-component SDW, two-component SC, and one-component CDW instabilities makes the fixed point $O(6)$ symmetric.[51]

The sign change in the superconducting $\Gamma^{s\pm}$ is the most notable effect within the parquet RG flow. Its physics originates in the effective "attraction" between SC and SDW fluctuations (not the order parameters!), namely from the fact that u_3, which is the attractive component of $\Gamma^{s\pm}$, gets the boost from u_1, which contributes to Γ^{SDW}. The boost is $4u_1u_3$ term in the r.h.s. of the RG equation for $\dot{u}_3$. This term overshadows the negative effect from u_2, u_4, and u_5, and as a result u_3 increases under RG. At the same time, intrapocket repulsions u_4 and u_5 decrease under RG. At some point, u_3^2 becomes lager compared to u_4u_5, and $\Gamma^{s\pm}$ becomes positive.

However, as we said earlier, parquet RG is only valid at energies above E_F. It is unlikely that the fixed point is reached above E_F, otherwise there would be at least pseudogap effects present above E_F, but there is no strong evidence for pseudogap in the pnictides. More likely, the couplings evolve under parquet RG (and $\Gamma^{s\pm}$ possibly changes sign at some scale) but u_i remain finite at E_F. To continue below this scale we need to derive a different set of equations, for which $u_i(E_F)$ serve as initial conditions.

C. RG flow below the scale of E_F

The RG equations below E_F for two-pocket model have been derived in Ref. 50 and we just quote the result. The most essential difference with the previous subsection concerns u_3 vertex, which contributes to both SC and SDW channels. Below E_F the structure of the external momenta becomes relevant, and one has to distinguish between $u_3^{(a)}$ with zero transferred momentum, $u_3^{(b)}$ with momentum transfer Q, and $u_3^{(c)}$ with zero total momentum (see Fig. 5). Each of the vertices now undergoes logarithmic renormalization in its own channel, crossed renormalizations no longer contribute because internal $E=O(E_F)$, and the arguments of the corresponding logarithms become $O(1)$. The new equations are

$$\dot{u}_3^{(a)} = 2u_1u_3^{(a)} - 2u_2u_3^{(a)},$$

$$\dot{u}_3^{(b)} = 2u_1u_3^{(b)},$$

$$\dot{u}_3^{(c)} = -[u_4+u_5]u_3^{(c)},$$

$$\dot{u}_4 = -[u_4^2 + (u_3^{(c)})^2],$$

$$\dot{u}_5 = -[u_5^2 + (u_3^{(c)})^2],$$

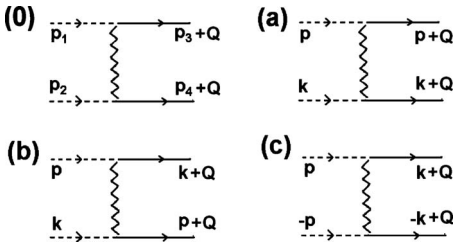

FIG. 5. (0) The u_3 vertex with general momenta p_1, p_2, p_3+Q, p_4+Q (all p_i are small and $p_1+p_2=p_3+p_4$). During calculations, three kinds of u_3 vertices arise-(a) the one with $p_1=p_3$, (b) the one with $p_2=p_3$, and (c) the one with $p_1+p_2=0$. The vertex "b" contributes to the renormalization in p-h channel, and the vertex "c" contributes to the renormalization in the p-p channel.

$$\dot{u}_1 = [u_1^2 + (u_3^{(b)})^2],$$

$$\dot{u}_2 = [2u_1u_2 - 2u_2^2], \tag{12}$$

where the derivatives are with respect to L. The effective vertices in the SDW and SC channels also get modified and become

$$\Gamma^{\mathrm{SDW}} = u_1 + u_3^{(b)},$$

$$\Gamma^{\pm} = \frac{-(u_4+u_5) + \sqrt{(u_4-u_5)^2 + 4(u_3^{(c)})^2}}{2}. \tag{13}$$

One can easily verify that new vertices satisfy

$$\frac{d\Gamma_i}{dL} = \Gamma_i^2 \tag{14}$$

as it should be because SC and SDW channels are now decoupled (no cross terms in RG equations).

The behavior of the vertices below E_F is illustrated in Figs. 6(b) and 6(c). If SC vertex is already positive (attractive) at E_F [Fig. 6(b)], it diverges at some scale below E_F, but for perfect nesting SDW vertex diverges first. Upon doping, SDW vertex levels off, and the first instability eventually becomes the SC one. If SC vertex remains negative at E_F [Fig. 6(c)], it decreases below E_F but still remains negative. In this situation, $s\pm$ SC does not appear even when SDW order gets killed by non-nesting.

To summarize: in a two-pocket model three scenarios are possible: (i) the instability occurs simultaneously in SDW, SC, and CDW channels, and a fixed point has $O(6)$ symmetry, (ii) SDW instability wins at prefect nesting, but yields to $s\pm$ superconductivity upon doping, and (iii) SDW instability exists near perfect nesting, but no SC instability emerges when SDW order is suppressed by doping. For the cases (i) and (ii), the SC gap has a simple plus-minus form, i.e., the gaps along hole and electron FSs are angle independent (up to $\cos 4\phi$ terms which we neglected) and are of the opposite signs.

The two-pocket model is indeed only a toy model for the pnictides. The actual band structure of the pnictides includes two electron FSs and at least two hole FSs. The question we now address is whether qualitatively new behavior emerges

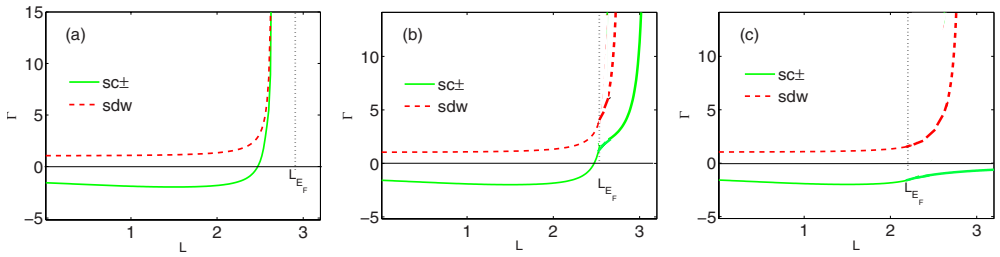

FIG. 6. (Color online) Running vertices in SDW and SC $s\pm$ channel for the two-pocket case at perfect nesting as functions of L. Three qualitatively different scenarios are possible: (a) vertices diverge before L_{E_F} is reached. Both vertices flow to the same fixed point, their ratio tends to one, and the fixed point has an extended symmetry. (b) L_{E_F} is reached before the fixed point but in the range of L where the SC vertex is already attractive (positive). The vertices flow independent of each other beyond L_{E_F} (below E_F), the SDW vertex diverges first. On doping SDW yields to SC (see Fig. 2). (c) The value L_{E_F} is reached when SC vertex is still repulsive (negative). In this case SC instability does not occur even after SDW instability is eliminated by doping.

when we increase the number of pockets. We argue below that there are new features not present in a two-pocket model.

IV. FOUR-POCKET MODEL

We now consider the case of two hole and two electron FSs. We neglect k_z variation in the FSs and consider a cross section in XY plane. The two electron FSs are generally ellipses, centered at $(0,\pi)$ and $(\pi,0)$ in the unfolded zone. The two hole FSs are circles centered at (0,0). They generally are of nonequal sizes, and one is less nested with electron FSs than the other.

The RG analysis of a generic four-pocket model is straightforward but rather cumbersome. We show the results in the two more easily trackable limits: one when the two hole FSs are completely equivalent, and the other when one of the two hole FSs is much weakly coupled with electron than the other one and can be neglected. In the second limit, four-pocket model reduces to three-pocket model.[28,57] We show that the system behavior is identical in the two limits, and make a conjecture that it doesn't evolve between the limits. We continue with our earlier assumption of circular electron FSs that nests with the hole FS. We begin with the limit when one hole FS can be neglected and four-pocket model reduces to three-pocket model.

A. Effective model with one hole at (0,0)

The interaction Hamiltonian for the four-pocket model is

$$\begin{aligned}\frac{m}{2\pi}H_{int} &= \sum u_1^{(1)}\ c^\dagger_{p_1 s} f^\dagger_{1p_2 s'} f_{1p_4 s'} c_{p_3 s} \\ &+ \sum u_2^{(1)}\ c^\dagger_{p_1 s} f^\dagger_{1p_2 s'} c_{p_4 s'} f_{1p_3 s} \\ &+ \sum \frac{u_3^{(1)}}{2}(c^\dagger_{p_1 s} c^\dagger_{p_2 s'} f_{1p_4 s'} f_{1p_3 s} + \text{H.c.}) \\ &+ f_1 \leftrightarrow f_2 \quad \text{and} \quad u_i^{(1)} \leftrightarrow u_i^{(2)} \\ &+ \sum \frac{u_5}{2} c^\dagger_{p_1 s} c^\dagger_{p_2 s'} c_{p_4 s'} c_{p_3 s} \\ &+ \sum \frac{u_4^{(1)}}{2} f^\dagger_{1p_1 s} f^\dagger_{1p_2 s'} f_{1p_4 s'} f_{1p_3 s} \\ &+ \sum \frac{u_4^{(2)}}{2} f^\dagger_{2p_1 s} f^\dagger_{2p_2 s'} f_{2p_4 s'} f_{2p_3 s} \\ &+ \sum u_6\ f^\dagger_{1p_1 s} f^\dagger_{2p_2 s'} f_{2p_4 s'} f_{1p_3 s} \\ &+ \sum u_7\ f^\dagger_{1p_1 s} f^\dagger_{2p_2 s'} f_{1p_4 s'} f_{2p_3 s} \\ &+ \sum \frac{u_8}{2}(f^\dagger_{1p_1 s} f^\dagger_{1p_2 s'} f_{2p_4 s'} f_{2p_3 s} + \text{H.c.}) \end{aligned} \quad (15)$$

This is a straightforward generalization of the two-pocket case (see also Ref. 57). The notations are the same as for the two-pocket model, but now f_1 and f_2 refer to fermions from the two different electron bands. The new terms u_6, u_7, and u_8 are different interpocket interactions between f fermions. Because we now have two different sets of electron state, it is convenient to work in the unfolded BZ, and in Fig. 7 we show the interactions that contribute to the pairing vertex. There are, however, subtle effects related to the actual, As-induced differences between folded and unfolded zones, and we will discuss them below.

The two electron bands are related by symmetry $k_x \leftrightarrow k_y$ [i.e., $\varepsilon_{f_1}(k_x,k_y)=\varepsilon_{f_2}(k_y,k_x)$], and it is natural to set $u_i^{(1)}=u_x^{(i)}=u_i$ (i runs between 1 and 4). We verified that no new terms

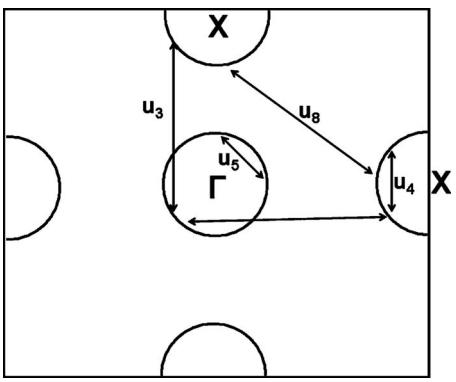

FIG. 7. Hole (center) and electron (edges) FSs in the unfolded BZ for four-pocket model. The arrows with symbols indicate various intrapocket and interpocket interactions which contribute to the SC vertex. There exist other density-density and exchange interpocket interactions (u_1, u_2, u_6, and u_7 terms, not shown).

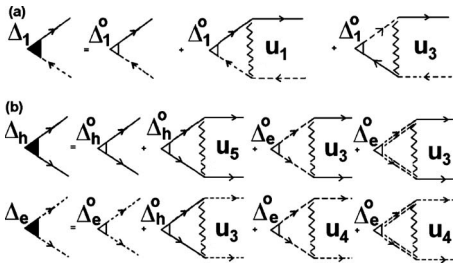

FIG. 8. The diagrams for the SDW and SC vertices for the four-pocket model [panels (a) and (b)]. The notations are the same as in Fig. 4. Single and double dashed lines describe fermions from the two electron bands.

are generated under RG flow, however the interactions between electron pockets must be included as they anyway are generated by RG.

The angular dependence of the vertices is incorporated in the same manner as described in Sec. II, by including $\alpha \cos 2\phi$ terms into the vertices which involve fermions near electron pockets. To simplify calculations, we first neglect the angular dependence of the intrapocket electron-electron interaction u_4. Later we show that including angular dependence of u_4 will not change the results qualitatively.

1. Vertices

The computational procedure is the same as before. We introduce infinitesimally small SC and SDW vertices, dress them up by the interactions, and express the renormalized vertices in terms of the running couplings.

The diagrammatic expressions for the renormalized vertices are presented in Fig. 8. For the SDW vertex we have $\Delta^{\mathrm{SDW}}=\Delta_1^{\mathrm{SDW}}+\Delta_2^{\mathrm{SDW}} \cos 2\phi$, ϕ being the angle along the electron FS. For SC vertex on the hole FS $\Delta^{\mathrm{SC}}=\Delta_h$ and on the two electron FSs $\Delta^{\mathrm{SC}}=\Delta_e \pm \bar{\Delta}_e \cos 2\phi$, as required by symmetry for an s-wave gap. If $|\bar{\Delta}_e|>|\Delta_e|$, the SC gap has nodes along the FS. The nodes are accidental in the sense that they are not protected by any symmetry.

For the SC vertex we then obtain the coupled set of equations

$$\begin{pmatrix} 1-u_5L & -2u_3L & -2\alpha u_3 L \\ -u_3L & 1-\tilde{u}_4L & 0 \\ -2\alpha u_3 L & 0 & 1 \end{pmatrix} \begin{pmatrix} \Delta_h^o \\ \Delta_e^o \\ \bar{\Delta}_e^o \end{pmatrix} = \begin{pmatrix} \Delta_h \\ \Delta_e \\ \bar{\Delta}_e \end{pmatrix}, \quad (16)$$

where $\tilde{u}_4=u_4+u_8$. For the SDW vertex we obtain (assuming that $\Delta_{1,2}$ are real)

$$\begin{pmatrix} 1+(u_1+u_3)L & \frac{\alpha}{2}(u_1+u_3)L \\ \alpha(u_1+u_3)L & 1 \end{pmatrix} \begin{pmatrix} \Delta_1^o \\ \Delta_2^o \end{pmatrix} = \begin{pmatrix} \Delta_1 \\ \Delta_2 \end{pmatrix}. \quad (17)$$

We included angular dependence of both u_3 and u_1 terms and for simplicity set α to be the same for both. Observe that α-dependent terms appear in SDW vertex with extra 1/2 compared to SC vertex. This is because internal and external part of the SDW vertex each contains one fermion from the electron FS, while in the SC vertex there are two such fermions, either in the internal or in the external part. One can easily check that in the SC vertex all α terms then appear with extra factor of 2 compared to SDW vertex.

The effective vertices are found by diagonalizing these matrices and casting the results into the forms $\Delta_i=\Delta_i^o(1+\Gamma_i L)$. For $\alpha=0$, the formulas simplify and we have

$$\Gamma_1^{\mathrm{SC}}=\Gamma^{s\pm}=\frac{-(\tilde{u}_4+u_5)+\sqrt{(\tilde{u}_4-u_5)^2+8(u_3)^2}}{2},$$

$$\Gamma_2^{\mathrm{SC}}=\Gamma^{s++}=\frac{-(\tilde{u}_4+u_5)-\sqrt{(\tilde{u}_4-u_5)^2+8(u_3)^2}}{2},$$

$$\Gamma^{\mathrm{SDW}}=\Gamma_1^{\mathrm{SDW}}=u_1+u_3. \quad (18)$$

The solutions corresponding to Γ_1 and Γ_2 are $\Delta_h/\Delta_e<0$ and $\Delta_h/\Delta_e>0$, accordingly, hence the notations $\Gamma^{s\pm}$ and Γ^{s++}. The vertex Γ^{s++} is repulsive for all couplings while $\Gamma^{s\pm}$ is repulsive for $2u_3^2<\tilde{u}_4u_5$ and is attractive for $2u_3^2>\tilde{u}_4u_5$. The SDW vertex is attractive. We recall that u_4 and u_5 are Coulomb interactions at small momentum transfer, while u_3 and u_8 are Coulomb interactions at large momentum transfer and are supposed to be smaller than u_5, u_4. At the bare level then there is no attractive component of Γ^{SC} for $\alpha=0$.

At a finite α we obtain two SDW vertices $\Gamma_1^{\mathrm{SDW}}=(u_1+u_3)(1+\sqrt{1+2\alpha^2})/2$ and $\Gamma_2^{\mathrm{SDW}}=-(u_1+u_3)(\sqrt{1+2\alpha^2}-1)/2$. The second one is repulsive, which the first one is attractive and only increases with α. For the SC vertex, the three Γ_i^{SC} are obtained by diagonalizing Eq. (16) what requires solving the cubic equation. The analytical expressions for Γ_i^{SC} are long and we refrain from presenting them (we will show all three Γ_i^{SC} in the figures). It is essential, however, that for *any* $\alpha\neq 0$, one of three Γ_i^{SC} is attractive even when $\tilde{u}_4u_5$ is larger than $2u_3^2$ and at $\alpha=0$ SC vertices are repulsive. At small α, we have for such induced solution

$$\Gamma_1^{\mathrm{SC}}=\alpha^2\left[\frac{4u_3^2u_5}{\tilde{u}_4u_5-2u_3^2}\right], \quad \tilde{u}_4u_5>2u_3^2. \quad (19)$$

Other two solutions $\Gamma_{2,3}^{\mathrm{SC}}$ are negative, i.e., repulsive.

For $\tilde{u}_4u_5<2u_3^2$, the attractive solution exists already at $\alpha=0$, and is only weakly affected by α. For $\tilde{u}_4u_5<2u_3^2$ we have

$$\Gamma_1^{\mathrm{SC}}=\Gamma^{s\pm}\left\{1+\alpha^2\left[\frac{2u_3^2(-\Delta u+\sqrt{(\Delta u)^2+8u_3^2})}{(\Gamma^{s\pm})^2\sqrt{(\Delta u)^2+8u_3^2}}\right]\right\}, \quad (20)$$

where $\Delta u=\tilde{u}_4-u_5$ and $\Gamma^{s\pm}$ is given by Eq. (18). The other two $\Gamma_{2,3}^{\mathrm{SC}}$ are again negative. We now proceed with the RG flow.

2. RG flow between Λ and E_F

Like in two-pocket case, at $\Lambda>E>E_F$, renormalizations in p-h and p-p channels are logarithmical and independent of the location of external momenta. The derivation of parquet RG equations is straightforward but requires more efforts as there are new terms in the Hamiltonian. For illustration, we show in Fig. 9 the diagrams contributing to the renormaliza-

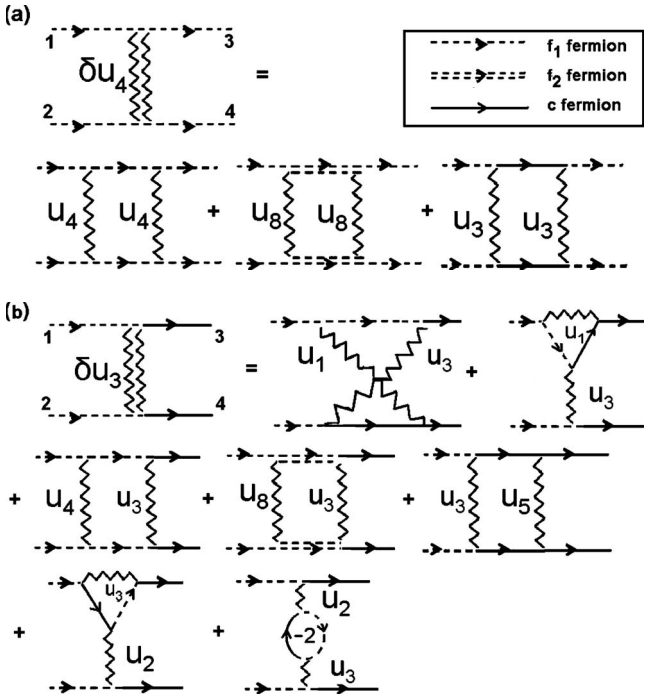

FIG. 9. Second-order diagrams for the renormalizations of u_4 and u_3 vertices [panels (a) and (b), respectively]. The combinatorial factors are not shown but must indeed be included.

tion of the vertices u_4 and u_3. The diagrams for the renormalization of other vertices are similar.

Collecting the diagrams for the renormalization of all couplings, we find that the terms $u_6 \pm u_7$ and $u_4 - u_8$ are decoupled from the rest of the terms and are renormalized as $\dot{u}_j = -(u_j)^2$, Because all these u_j are the differences between Coulomb interactions at small and large momentum transfers, their bare values are positive in which case the these interactions flow to zero under RG and are therefore irrelevant.

The other five vertices are all coupled and flow according to

$$\dot{u}_5 = -[u_5^2 + 2u_3^2],$$

$$\dot{\tilde{u}}_4 = -[\tilde{u}_4^2 + 2u_3^2],$$

$$\dot{u}_1 = +[u_1^2 + u_3^2],$$

$$\dot{u}_2 = +[2u_1u_2 - 2u_2^2]$$

$$\dot{u}_3 = +[4u_1u_3 - 2u_2u_3 - u_5u_3 - \tilde{u}_4u_3]. \quad (21)$$

This set of equations can be easily solved numerically. Figure 10 shows the plot of u_5/u_1, $\tilde{u}_4/u_1$, u_2/u_1, and u_3/u_1 with L. For simplicity, we set bare values of $\tilde{u}_4$ and u_5 to be equal—the two then remain equal in the process of RG flow. The values of the ratios at the fixed point are indicated by the dots. These can be easily found analytically by requesting that all five equations in Eq. (21) be identical. Imposing this condition we obtain $u_5/u_1 = \tilde{u}_4/u_1 = -\sqrt{6} \approx -2.45, u_3/u_1 = (3 + 2\sqrt{6})^{1/2} \approx 2.81, u_2/u_1 = 0$. Like in two-pocket model, intrapocket repulsions $\tilde{u}_4$ and u_5 decrease under RG, change

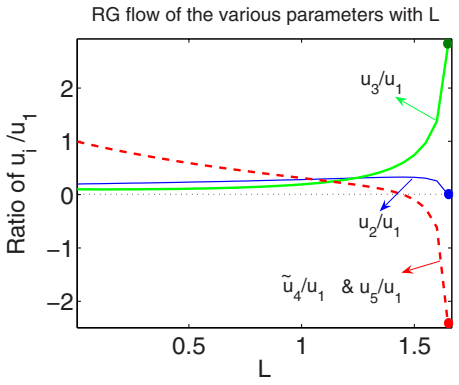

FIG. 10. (Color online) The solution of Eq. (21)—the RG flow of u_5, $\tilde{u}_4$, u_2, and u_3 (all relative to u_1) with L. For simplicity, we set bare values of $\tilde{u}_4$ and u_5 equal. Note how, as fixed point is approached, the renormalized Coulomb repulsion at small momenta (u_5 and $\tilde{u}_4$ terms) is suppressed and eventually changes sign, while the pair hopping term u_3 is strengthened.

sign at some value of L, and become negative at larger L. This sign change (overscreening) goes beyond a conventional McMillan-Tolmachev screening of the Coulomb interaction, and is the result of the push from u_3, which in turn increases under RG due to the push from u_1 which contributes to the SDW vertex. So, eventually, overscreening is the result of the attraction between SDW and SC fluctuations. The difference $\tilde{u}_4 u_5 - 2u_3^2$ also changes sign at some L and becomes negative at larger L.

We now substitute the running couplings into the expressions for SC and SDW vertices and check how they flow. The results are presented in Fig. 11 for $\alpha = 0.4$. For the SDW vertices, the positive one increases with L, like in the two-pocket model, while the negative one becomes more negative, i.e., even less relevant. For the SC vertices, Γ_1^{SC} is positive for all L, the other two $\Gamma_{2,3}^{SC}$ are negative and hence irrelevant. The positive Γ_1^{SC} interpolates between Eq. (19) at small L, and Eq. (20) at larger L. We emphasize that for all values of L this is the same solution, i.e., there is no level crossing (see Fig. 11).

In Fig. 12(a) we compare the behavior of Γ^{SDW} and Γ^{SC} as functions of L assuming that the fixed point is reached at energies above E_F. At small L, we have the same situation as in two-pocket model: SDW vertex is larger than SC vertex. However, the rate of increase in the SC vertex exceeds that of the SDW vertex, and at some L before the fixed point is reached, Γ^{SC} *crosses over* Γ^{SDW} implying that superconductivity becomes the leading instability even at perfect nesting. Such crossing has been reported in fRG calculations[27] for the same model. We view the agreement as a good indication that numerical fRG and analytical parquet RG approaches describe the same physics. In our analytical RG, the reason for the crossing is combinatoric: compared to two-pocket case (where SDW and SC vertices flow to the same value under RG), the presence of the second electron FS adds the factor of 2 to the renormalization of the SC vertex as a pair of fermions from the hole FS can hope to each of the two electron FSs. However, there is no such factor of 2 in the renormalization of the SDW vertex due to momentum conservation.

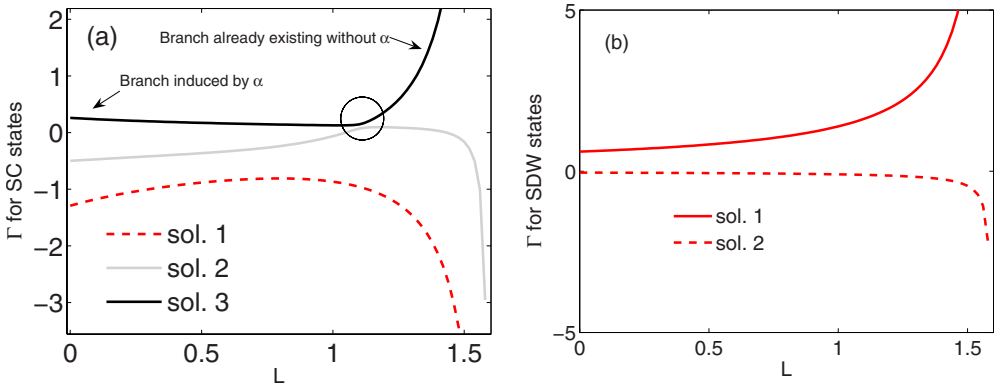

FIG. 11. (Color online) The flow of SC and SDW vertices under RG in the effective three-pocket model for $\alpha=0.4$. (a) Three SC vertices. One solution is attractive for all L (and corresponds to $s\pm$ pairing), the other two are repulsive. One of the repulsive solutions is of $s\pm$ character, another of $s{+}{+}$ character. At small L, the positive solution is the one induced by α, at large L it almost coincides with the solution which becomes positive for these L already at $\alpha=0$. The circle marks the area where positive and negative solutions come close to each other. The splitting between the two increases with α. (b) The two SDW vertices. One vertex is always attractive (positive) and the other is repulsive (negative).

We emphasize that the crossing of Γ_1^{SDW} and Γ_1^{SC} is not related to the angular dependence of the interaction. Even when $\alpha=0$, SC vertex exceeds SDW vertex near the fixed point of parquet RG. At the fixed point, the ratio of the two is $\Gamma_1^{\mathrm{SC}}/\Gamma_1^{\mathrm{SDW}}\approx 1.69$.

The SC order parameter by itself has an interesting character. We recall that we approximate the gap along the hole FS by a constant Δ_h and approximate the gap along the two electron FSs by $\Delta_e \pm \bar{\Delta}_e \cos 2\phi$. At small L, the attractive Γ^{SC} exists only because of a nonzero α, and $\bar{\Delta}_e$ is larger that Δ_e (Ref. 28), hence the gap along the two electron FSs has accidental nodes. As L increases, the SC vertex Γ evolves, according to Fig. 11, and eventually gets close to the would-be solution for $\alpha=0$. For the latter, $\bar{\Delta}_e=0$, and the gap obviously has no nodes. The crossover from one limit to the other is displayed in Fig. 13, where we show the flow of the gaps Δ_h, Δ_e, and $\bar{\Delta}_e$, corresponding to the leading SC vertex. For the value of α which we used in this figure ($\alpha=0.4$) the transition from nodal to nodeless gap occurs at L smaller than the one at which SC vertex crosses the SDW vertex, i.e., when SC becomes the leading instability, the superconducting gap is already nodeless. But for other values of α we can get either nodeless or nodal SC in this regime. In Fig. 14 we plot the "phase diagram" coming out of parquet RG for different α [the bare values of u_i are the same for all figures in this section]. In white region, SDW vertex is the largest and SC vertex is subleading, implying that superconductivity can be revealed only after SDW order is suppressed by doping. In the shaded region the SC vertex is the largest. We see that superconducting gap in this region can actually be either nodal or nodeless, depending on the value of α. At $\alpha=0$, the ratio of Δ_e and Δ_h at the fixed point is $\Delta_h=-\sqrt{2}\Delta_e$.

3. RG flow below the scale of E_F

We now consider the situation below E_F. As in the two-pocket model, we have to introduce three different u_3 couplings-$u_3^{(a)}$, $u_3^{(b)}$, and $u_3^{(c)}$ of which $u_3^{(b)}$ is the part of SDW vertex, and $u_3^{(c)}$ is the part of the SC vertex [the corresponding $u_3^{(i)}$ replace u_3 in Eqs. (16) and (17)]. The flow of the couplings is now governed by

$$\dot{u}_5 = -[u_5^2 + 2(u_3^{(c)})^2],$$

$$\dot{\tilde{u}}_4 = -[\tilde{u}_4^2 + 2(u_3^{(c)})^2],$$

$$\dot{u}_1 = +[u_1^2 + (u_3^{(b)})^2],$$

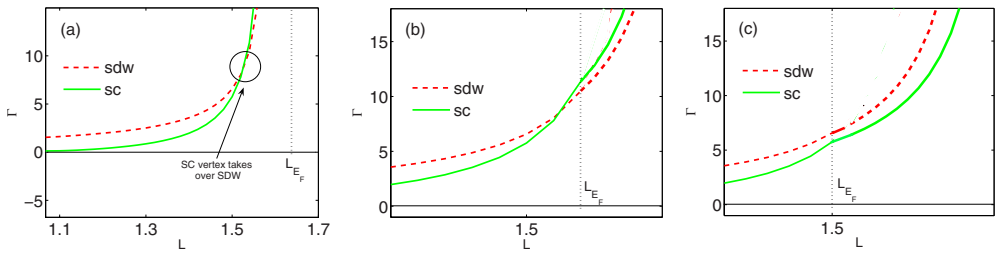

FIG. 12. (Color online) The flow of vertices for different values of L_{E_F} for $\alpha=0.4$. (a) RG flow reaches fixed point before L_{E_F}. SDW vertex is larger at small L but SC vertex "crosses" the SDW vertex at some distance from the fixed point and becomes the strongest vertex at the fixed point. As a result, the system develops a SC order. (b) L_{E_F} is reached after the 'crossing' but before reaching fixed point. The system still develops a SC order, and SDW order does not emerge. (c) L_{E_F} is reached before the crossing. In this case the SDW vertex still develops at small dopings, and SC order emerges at larger dopings, when SDW order gets suppressed.

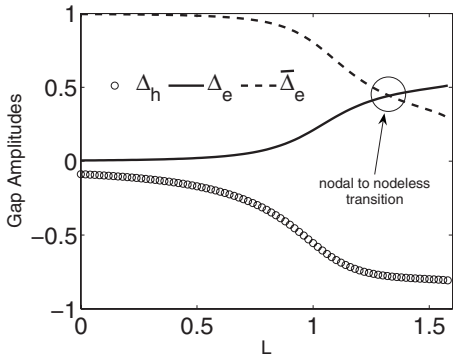

FIG. 13. The evolution of the three components of the superconducting gap with L for $\alpha=0.4$. Δ_h is the gap on the hole FS, and $\Delta_e \pm \bar{\Delta}_e \cos 2\phi$ are the gaps along electron FSs. A circle marks the point where Δ_e and $\bar{\Delta}_e$ cross, and the gap along each of electron FSs changes from nodal to nodeless. Note that the solution is always of s± character; meaning Δ_h and Δ_1^e are of opposite signs.

$$\dot{u}_2 = +[2u_1u_2 - 2u_2^2],$$

$$\dot{u}_3^{(a)} = 2u_1u_3^{(a)} - 2u_2u_3^{(a)},$$

$$\dot{u}_3^{(b)} = 2u_1u_3^{(b)},$$

$$\dot{u}_3^{(c)} = [u_5 + \tilde{u}_4]u_3^{(c)}. \tag{22}$$

Note the $\tilde{u}_4$ and u_5 have identical equations and hance treated identically. One can then straightforwardly verify using Eq. (22) that SC and SDW vertices decouple, as they should, and each satisfies $\dot{\Gamma}_i = \Gamma_i^2$. Hence, as before, whichever vertex is larger at E_F gives rise to the first instability as T decreases. If SC vertex prevails, the system becomes SC at perfect nesting and remains a SC at finite dopings [Fig. 12(b)]. If SDW vertex prevails, the system becomes an SDW antiferromagnet at perfect nesting and then eventually becomes a SC upon doping [Fig. 12(c)]. In distinction to the two-pocket case, we do not need to worry about the sign of the SC

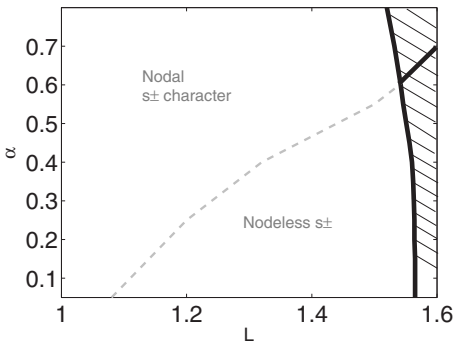

FIG. 14. The RG flow of the four-pocket model in variables α and L over the range of energies above E_F. The white zone is where SDW vertex is the largest, and the shaded zone is where SC $s\pm$ vertex is the largest. The thick solid line in the shaded zone marks the transition form nodal to nodeless s± gap in the region where SC vertex wins. The dashed line is the continuation of this transition line into the region where SDW vertex takes over.

vertex once SDW instability is reduced by doping because one of Γ^{SC} is always attractive (see Fig. 11). We emphasize again that this attractive Γ^{SC} leads to either nodeless $s\pm$ gap, or to $s\pm$ gap with nodes along the electron FSs, depending on α and on the interplay between E_F and the scale at which parquet RG flow reaches the fixed point.

4. Effect of the angular dependence of electron-electron interaction

For completeness, we present the results for the evolution of the SC gap structure under RG flow for the case when we preserve the angular dependence in the electron-electron interactions—u_4 and u_8 terms. These interactions only contribute to the pairing channel, so it will be sufficient co consider u_4 and u_8 interactions between fermions with momenta $k,-k;p,-p$. The generic structure of the angular dependence of such interactions is given by Eq. (6). We found earlier that u_4 and u_8 terms contribute to the s-wave pairing in the combination $\tilde{u}_4 = u_4 + u_8$, so we need to consider only this term. We have

$$\tilde{u}_4(k,p) = \tilde{u}_4[1 + 2\alpha'(\cos 2\phi_k \pm \cos 2\phi_p) \pm 4\alpha'' \cos 2\phi_k \cos 2\phi_p], \tag{23}$$

where plus sign is for intrapocket interaction and minus sign is for interpocket interaction.

There are two new effects associated with the angular dependence of $\tilde{u}_4(k,p)$. First, when $\tilde{u}_4 u_5 > 2u_3^2$, the pairing vertex Γ^{SC} not necessarily has an attractive component. It was always the case for angle-independent $\tilde{u}_4$. Now the existence of the attractive interaction is subject to condition $K>0$, where

$$K = 2\tilde{u}_4 u_5[(\alpha')^2 - \alpha''] + u_3^2(\alpha^2 + 2\alpha'' - 3\alpha\alpha'). \tag{24}$$

If we set the angular dependence of u_3 and $\tilde{u}_4$ terms to be equal, i.e., set $\alpha'=\alpha, \alpha''=0$, this condition reduces to $\tilde{u}_4 u_5 > u_3^2$, which is well satisfied. However, for a generic α' and α'', Eq. (24) is not necessarily satisfied, and if $K<0$, attractive Γ_1^{SC} appears only above some RG scale L, like in two-pocket model.

Second, the gap structure may change in some range of L. To demonstrate this, make angular dependence of u_3 and $\tilde{u}_4$ equal, i.e., set $\alpha'=\alpha, \alpha''=0$. The set of equations for the SC vertices then becomes

$$\begin{pmatrix} 1-u_5L & -2u_3L & -2\alpha u_3L \\ -u_3L & 1-\tilde{u}_4L & -\alpha\tilde{u}_4L \\ -2\alpha u_3L & -2\alpha\tilde{u}_4L & 1 \end{pmatrix} \begin{pmatrix} \Delta_h^o \\ \Delta_e^o \\ \bar{\Delta}_e^o \end{pmatrix} = \begin{pmatrix} \Delta_h \\ \Delta_e \\ \bar{\Delta}_e \end{pmatrix}. \tag{25}$$

As before, we need to diagonalize this set, cast the result in the form $\Delta_i = \Delta_i^o(1+\Gamma_i L)$ and consider the largest Γ_i. The evolution with L of Δ_h, Δ_e, and $\bar{\Delta}_e$ for such Γ_i is shown in Fig. 15, and the phase diagram is shown in Fig. 16. We see that, over some range when $\bar{\Delta}_e$ is the largest and the gap has nodes along the electron FSs, the gap actually has "*nodal s ++*" character in the sense that Δ_h and Δ_e are of the same sign, although the dominant term is still the oscillating component $\bar{\Delta}_e$. Note, however, that the character of the gap

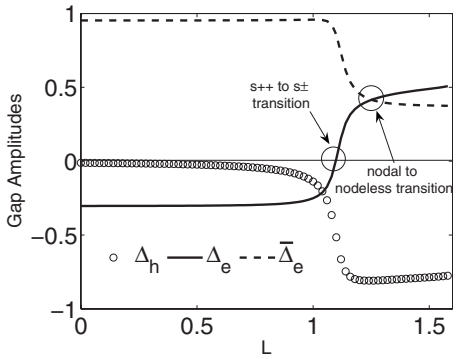

FIG. 15. Behavior of the different Δ's when the angular dependence of the electron intrapocket coupling u_4 is included. As before, we set α=0.4. The only difference compared to Fig. 13 is the appearance of the region, at small L, where SC order parameter has nodal s++ character meaning that Δ_h and Δ_e are of the same sign. In this range of L the SC vertex is, however, smaller than the SDW vertex. The character of the SC gap changes to nodal $s\pm$ and then to no-nodal $s\pm$ before SC vertex takes over SDW vertex.

changes back to $s\pm$ before it becomes nodeless.

This appearance of the nodal s++ like gap might seem unusual, but it should be kept in mind that this gap is present in the parameter range where without the angular dependence there would not have been a solution. The firm requirement then is that in the solution induced by α the oscillating $\bar{\Delta}_e$ component is the largest, because this is the way to minimize the effect of intrapocket Coulomb repulsion. The relative sign between the subleading Δ_h and Δ_e terms is not uniquely determined by this requirement and be either minus or plus, depending on the interplay between electron-hole and electron-electron interactions.

These two potential changes introduced by the angular dependence of $\tilde{u}_4$, however, affect only the behavior at small L. At large L (i.e., at low energies), the system behavior remains unchanged: SDW vertex is the largest at small/intermediate L, but SC vertex still crosses over SDW vertex at some L, and beyond this scale SC instability comes first.

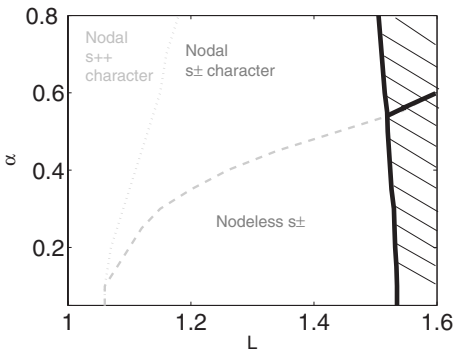

FIG. 16. Same as in Fig. 14 but with the angular dependence of the electron intrapocket coupling u_4 included. The only new feature is the existence of a range where SC vertex (secondary in this range to SDW vertex) has nodal s++ character meaning that the gaps along electron FSs have nodes, but the average value of the gap along the electron FS is of the same sign as the gap along the hole FS.

B. Four-pocket model in the limit when two hole FSs are identical

We now consider the opposite limit where the two hole FSs centered at (0,0) are equivalent. We show that the system behavior in this second limit is the same as in the first. The equivalence of the two limits hints that the system behavior in the intermediate case is very likely the same as in the two limits.

The computations in the case of two identical hole FSs proceed in the same way as before, but there are more vertices. The new terms are u_1, u_2, and u_3 interactions with hole fermions from the second hole bands, the analogs of these three interactions for fermions from the two hole bands, u_5 interaction for the second hole band, and the interactions of the kind $u_5^* \Sigma c_1^\dagger c_1^\dagger c_1 c_2$. Note that there are no $f_1^\dagger f_1^\dagger f_1 f_2$ terms for fermions from the two electron bands because they would violate momentum conservation.

The full set of RG equations is rather cumbersome but we verified that (i) RG flow indeed preserved the invariance between the two hole bands, and (ii) all intrapocket and interpocket interactions involving fermions from the hole bands flow to the same value u_5. The analysis based on five-orbital Hubbard model also yields near-equivalence of all u_i involving fermions from hole pockets.[56]

To simplify the presentation we set all interactions involving fermions near hole FSs to be equal to u_5 from the start and also neglect the angular dependence of the interactions. We also set $u_4 = u_8$ because $u_4 - u_8 > 0$ again flows to zero under RG [see paragraph before Eq. (21)].

1. Vertices

The equations for the SC and SDW vertices are obtained in the same way as before (see Fig. 8), but now Δ_h is composed from fermions with k and $-k$ belonging to either of the two hole pockets. This leads to the equations for the SDW vertex Δ_1 and SC vertices Δ_h and Δ_e in the form

$$\Delta_1 = \Delta_1^o (1 + \tilde{u}_1 + \tilde{u}_3) \tag{26}$$

and

$$\begin{pmatrix} 1 - \tilde{u}_5 L & -\tilde{u}_3 L \\ -2\tilde{u}_3 L & 1 - \tilde{u}_4 L \end{pmatrix} \begin{pmatrix} \Delta_h^o \\ \Delta_e^o \end{pmatrix} = \begin{pmatrix} \Delta_h \\ \Delta_e \end{pmatrix}, \tag{27}$$

where $\tilde{u}_1 = 2u_1$, $\tilde{u}_3 = 2u_3$, $\tilde{u}_4 = 2u_4$, and $\tilde{u}_5 = 4u_5$. Casting the results into $\Delta_i = \Delta_i^o (1 + \Gamma_i L)$, we obtain

$$\Gamma^{\mathrm{SDW}} = \tilde{u}_1 + \tilde{u}_3,$$

$$\Gamma^{s\pm} = \frac{-(\tilde{u}_4 + \tilde{u}_5) + \sqrt{(\tilde{u}_4 - \tilde{u}_5)^2 + 8(\tilde{u}_3)^2}}{2}. \tag{28}$$

2. Parquet RG equations

The RG equations are obtained in the same way as before and are

$$\dot{\tilde{u}}_5 = -[\tilde{u}_5^2 + 2\tilde{u}_3^2],$$

$$\dot{\tilde{u}}_4 = -[\tilde{u}_4^2 + 2\tilde{u}_3^2],$$

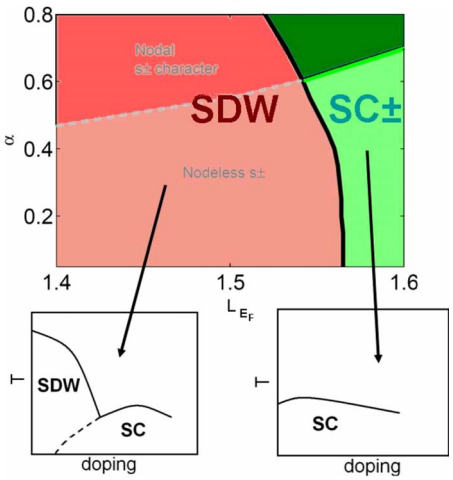

FIG. 17. (Color online) The phase diagram of the four-pocket model at perfect nesting in variables α and $L_{E_F}=\log \Lambda/E_F$. To the left (red) is the region where SDW order develops, and to the right (green) is the region of the SC order. Dark and light regions correspond to nodal (dark) and nodeless (light) SC gap along the electron FSs. The two subfigures show the behavior at finite doping. Superconducting state, which is brought out upon doping, in the left subfigure is either nodeless or nodal depending on whether the system is in the dark or in the light region. The transition between SDW and SC states can be either first order or involve intermediate coexistence phase (Refs. 58 and 59).

$$\dot{\tilde{u}}_1 = +[\tilde{u}_1^2 + \tilde{u}_3^2],$$

$$\dot{\tilde{u}}_3 = +[4\tilde{u}_1\tilde{u}_3 - \tilde{u}_5\tilde{u}_3 - \tilde{u}_4\tilde{u}_3]. \quad (29)$$

We drop u_2 for simplicity as it eventually becomes smaller than other u_i

Comparing these equations and the equations for the vertices with those for one hole FS [Eqs. (18) and (21)] we see that they are identical up to renormalizations $u_i \to \tilde{u}_i$. Accordingly, the flow of the couplings and the vertices is the same as in the limit when only one hole FS is present. In both limits, SC vertex is secondary to SDW vertex at large energies, but has larger slope and crosses over SDW vertex at some energy, before the system reaches a fixed point. At smaller energies, SC vertex is larger, i.e., if parquet RG flow extends beyond the scale where the two vertices cross, the system first develops a SC order even at perfect nesting. This SC order can be either with or without nodes in the gaps along the two electron FSs (see Fig. 17). The only difference to the effective three-pocket model is that now at the fixed point we have $\Delta_e = -\sqrt{2}\Delta_h$ for $\alpha=0$ as opposed to $\Delta_h = -\sqrt{2}\Delta_e$ for the earlier case.

As we said, the equivalence of the system behavior in the two limits strongly suggests that the same behavior holds also in the intermediate case.

C. Summary of the results for the four-pocket model

Collecting all the points we have discussed—we have shown that under suitable extent of renormalization of the Coulomb repulsion and pair-hopping couplings one can have

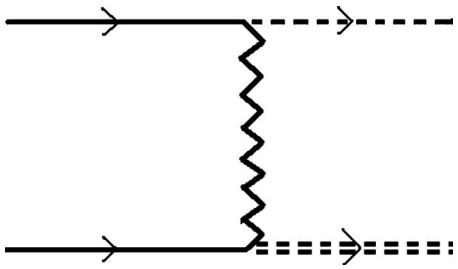

FIG. 18. The scattering which takes two fermions from the region near $k=0$ and scatters them to fermions with momenta near $(\pi,0)$ and $(0,\pi)$. This process is not allowed in the unfolded BZ because of momentum nonconservation, but it is allowed as an umklapp process in the folded BZ, which knows about As.

SDW, nodal $s\pm$, and nodeless $s\pm$ state even at perfect nesting. The angular dependence of the interaction between holes and electrons tends to drive the system toward a nodal SC phase. The SC order develops if the fixed point is reached within parquet RG, but if the scale E_F is reached before that, the system develops either SDW or SC order (either nodeless or nodal), depending on at what L the flow crosses over from parquet to ladder RG. That the SC $s\pm$ order can emerge even at perfect nesting is specific feature of the four-pocket model. This feature was not present in the two-pocket model, where the fixed point had an $O(6)$ symmetry. This symmetry is clearly broken in the four-pocket model, even when $\alpha=0$. The "crossing" of the SDW and SC vertices can be unambiguously attributed to the presence of the other electron pocket because its presence helps SC but not SDW.

Figure 17 summarizes the implication of our results toward the actual phase diagrams of Fe pnictides. In the SDW dominated region (red), SC emerges after doping reduces SDW order. In the other part (green) where SC dominates, SC order prevails already at perfect nesting. The $s\pm$ SC gap can be nodeless or have nodes along electron FSs depending on how strong is the angular dependence of the interaction between electrons and holes. Nodal regions are shown in dark color, and again this will be visible only after getting rid of SWD state by doping.

A final remark: in the analysis above we considered only the interactions which obey momentum conservation in the unfolded BZ. These are direct interactions between fermionic states obtained by the hybridization of 5 Fe orbitals. There exists, however, additional interactions which involve pnictide orbitals as intermediate states. These additional interactions obey momentum conservation in the folded BZ but they do not always obey momentum conservation in the unfolded, Fe-only BZ. An example of such process is shown in Fig. 18: two fermions from the hole band near $k=0$ scatter into two fermions at two *different* electron pockets. In the unfolded zone, this process does not conserve momentum, and we did not include it into our consideration. In the folded zone, both electron FSs are at (π,π), and this process is an umklapp process. The difference is indeed due to the fact that in reality such process involves intermediate states on As.

Neither our RG procedure nor fRG calculations include such terms. How important are they is not known. On general grounds, such interactions tend to enhance the SDW

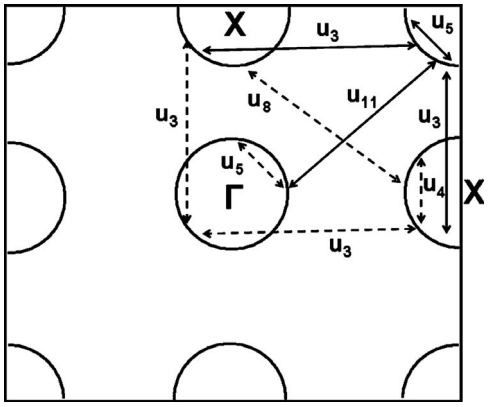

FIG. 19. The FSs and interactions in the five-pocket model. Dashed lines mark the interactions already present in four-pocket model, solid lines mark the new pairing interactions specific to five-pocket model. As before, we only present interactions which contribute to the pairing vertices. There are other density-density and exchange interactions between electrons belonging to different pockets.

vertex and might potentially alter the picture that we presented. They also may alter the ordering momentum of the SDW state. This remains an open issue.

V. FIVE-POCKET MODEL

We now extend the analysis from previous two sections to a five-pocket model in which we include into consideration the additional hole pocket appearing at (π,π) point in the unfolded BZ. We show below that the behavior of five-pocket model is similar to that for two-pocket model in the sense that SDW vertex exceeds SC vertex along the whole RG trajectory, and SDW and SC vertices tend to the same value if the fixed point is reached within parquet RG.

FIG. 20. The new interaction vertices for the five-pocket model. Single and double solid lines denote fermions from the two hole pockets, single and double dashed lines denote fermions from the two electron pockets.

As in the previous section, we restrict our consideration to the two limits, one when the two hole FSs centered at (0,0) are identical, and the other when one of these two hole FSs is relatively weakly coupled to electronic states and can be neglected. In the latter case, five-pocket model reduces to an effective four-pocket model consisting of one hole FS at (0,0), one hole FS at (π,π), and the two electron FSs at $(0,\pi)$ and $(\pi,0)$. We show that the system behavior is again identical in the two limits.

A. Effective model with one hole pocket at (0,0)

The FS geometry and interactions contributing to the SC vertex for the effective four-pocket model with hole pockets at (0,0) and (π,π) are presented in Fig. 19

The Hamiltonian now contains three new terms u_9, u_{10}, and u_{11}, which are density-density, exchange, and pair-hopping interaction between fermions belonging to two different hole pockets. In addition, we have three new vertices shown in Fig. 20. These include fermions from two different hole and two different electron FSs. We call them w_i vertices (i runs from 1 to 3).

The Hamiltonian now has the form

$$\frac{m}{2\pi}H_{int} = \sum u_1^{(1)}\ c^\dagger_{1p_1s} f^\dagger_{1p_2s'} f_{1p_4s'} c_{1p_3s} + \sum u_2^{(1)}\ c^\dagger_{1p_1s} f^\dagger_{1p_2s'} c_{1p_4s'} f_{1p_3s} + \sum \frac{u_3^{(1)}}{2}(c^\dagger_{1p_1s} c^\dagger_{1p_2s'} f_{1p_4s'} f_{1p_3s} + \text{H.c.})$$
$$+ f_1 \leftrightarrow f_2 \text{ (with } c_1 \text{ unchanged) and } u_i^{(1)} \leftrightarrow u_i^{(2)} + c_1 \leftrightarrow c_2 \text{ (with } f_1 \text{ unchanged) and } u_i^{(1)} \leftrightarrow u_i^{(3)}$$
$$+ c_1 \leftrightarrow c_2 \text{ (with } f_2 \text{ unchanged) and } u_i^{(2)} \leftrightarrow u_i^{(4)} + \sum \frac{u_4^{(1)}}{2} f^\dagger_{1p_1s} f^\dagger_{1p_2s'} f_{1p_4s'} f_{1p_3s} + \sum \frac{u_4^{(2)}}{2} f^\dagger_{2p_1s} f^\dagger_{2p_2s'} f_{2p_4s'} f_{2p_3s}$$
$$+ \sum \frac{u_5^{(1)}}{2} c^\dagger_{1p_1s} c^\dagger_{1p_2s'} c_{1p_4s'} c_{1p_3s} + \sum \frac{u_5^{(2)}}{2} c^\dagger_{2p_1s} c^\dagger_{2p_2s'} c_{2p_4s'} c_{2p_3s} + \sum u_6\ f^\dagger_{1p_1s} f^\dagger_{2p_2s'} f_{2p_4s'} f_{1p_3s} + \sum u_7\ f^\dagger_{1p_1s} f^\dagger_{2p_2s'} f_{1p_4s'} f_{2p_3s}$$
$$+ \sum \frac{u_8}{2}(f^\dagger_{1p_1s} f^\dagger_{1p_2s'} f_{2p_4s'} f_{2p_3s} + \text{H.c.}) + c \leftrightarrow f \text{ and } (u_6,u_7,u_8) \leftrightarrow (u_9,u_{10},u_{11}) + \sum w_1\ c^\dagger_{1p_1s} f^\dagger_{1p_2s'} f_{2p_4s'} c_{2p_3s}$$
$$+ \sum w_2\ c^\dagger_{1p_1s} f^\dagger_{1p_2s'} c_{2p_4s'} f_{2p_3s} + \sum \frac{w_3}{2} c^\dagger_{1p_1s} c^\dagger_{2p_2s'} f_{1p_4s'} f_{2p_3s} + (1 \leftrightarrow 2)\ldots \tag{30}$$

The analysis of the five-pocket model parallels that of the four-pocket model, so we will be rather brief and present only the results. We verified that RG equations for u_4, u_5, u_8 and u_{11} are identical, and these four couplings tend to the

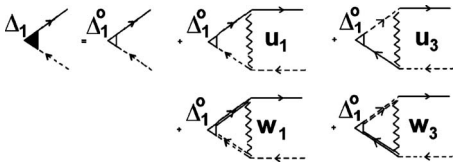

FIG. 21. The diagrammatic equation for the renormalized SDW vertex in the five-pocket model. Comparing with the corresponding Fig. 8(a) for the four-pocket case, there are extra diagrams which contribute to the SDW vertex. This leads to effectively doubling Γ^{SDW}.

same value at the fixed point. To make the presentation compact, we set $u_4=u_5=u_8=u_{11}$ from the start and call all of them u_4. Similarly we set $u_6=u_7=u_9=u_{10}$ calling it u_6. It is convenient to introduce $\tilde{u}_i=u_i+w_i$ $(i=1-3)$, and $\tilde{\tilde{u}}_i=u_i-w_i$. We will use these variables below.

1. Vertices

We first consider the case when the interactions are angle-independent ($\alpha=0$) and then discuss system behavior at a nonzero α. The SC and SDW vertices are obtained in the same way as before, but there are additional terms for the SDW term due to w_i vertices (see Fig. 21). Combining this with the equations for the SC vertices at (0,0) and (π,π) (Δ_{h1} and Δ_{h2}, respectively) we obtain

$$\begin{pmatrix} 1-2u_4L & -u_3L & -u_3L \\ -2u_3L & 1-u_4L & -u_4L \\ -2u_3L & -u_4L & 1-u_4L \end{pmatrix} \begin{pmatrix} \Delta_e^o \\ \Delta_{h1}^o \\ \Delta_{h2}^o \end{pmatrix} = \begin{pmatrix} \Delta_e \\ \Delta_{h1} \\ \Delta_{h2} \end{pmatrix} \tag{31}$$

and

$$\Delta_1 = \Delta_1^o[1+(\tilde{u}_1+\tilde{u}_3)L] \tag{32}$$

(we recall that we set $u_4=u_5$). Casting the equations for the SC vertices in the form $\Delta_i=\Delta_i^o(1+\Gamma_i)$ and neglecting repulsive vertex for s++ SC, we obtain

$$\Gamma^{\mathrm{SDW}} = \tilde{u}_1 + \tilde{u}_3,$$

$$\Gamma^{s\pm} = -2u_4 + \tilde{u}_3 + \tilde{\tilde{u}}_3. \tag{33}$$

Note that SDW and SC vertices contain different terms involving u_3. The gap structure for the SC vertex $\Gamma^{s\pm}$ is $\Delta_{h1}=\Delta_{h2}=-\Delta_e$.

2. RG flow between Λ and E_F

The set of parquet RG equations is obtained in the same way as before. Collecting the equations for the other variables we obtain

$$\dot{\tilde{u}}_1 = \tilde{u}_1^2 + \tilde{u}_3^2,$$

$$\dot{\tilde{u}}_2 = 2\tilde{u}_1\tilde{u}_2 - 2\tilde{u}_2^2,$$

$$\dot{\tilde{u}}_3 = 4\tilde{u}_1\tilde{u}_3 - 2\tilde{u}_2\tilde{u}_3 - 2\tilde{u}_3(u_4+u_6) - 2\tilde{\tilde{u}}_3(u_4-u_6),$$

$$2\dot{u}_6 = -(2u_6)^2 - (\tilde{u}_3-\tilde{\tilde{u}}_3)^2,$$

$$2\dot{u}_4 = -(2u_4)^2 - (\tilde{u}_3+\tilde{\tilde{u}}_3)^2,$$

$$\dot{\tilde{\tilde{u}}}_3 = 4\tilde{\tilde{u}}_1\tilde{\tilde{u}}_3 - 2\tilde{\tilde{u}}_2\tilde{\tilde{u}}_3 - 2\tilde{\tilde{u}}_3(u_4+u_6) - 2\tilde{u}_3(u_4-u_6),$$

$$\dot{\tilde{\tilde{u}}}_1 = \tilde{\tilde{u}}_1^2 + \tilde{\tilde{u}}_3^2,$$

$$\dot{\tilde{\tilde{u}}}_2 = 2\tilde{\tilde{u}}_1\tilde{\tilde{u}}_2 - 2\tilde{\tilde{u}}_2^2. \tag{34}$$

This set of equations almost decouples between the subsets for $\tilde{u}_i$ and $\tilde{\tilde{u}}_i$, the only places where the two subsets mix are the equations for the flow of u_4 and u_6 whose r.h.s. contains both $\tilde{u}_3$ and $\tilde{\tilde{u}}_3$. Rewriting this set as equations for the ratios of the couplings, we found four fixed points. One corresponds to $\tilde{\tilde{u}}_i$ vanishing compared to $\tilde{u}_i$, another to $\tilde{u}_i$ vanishing compared to $\tilde{\tilde{u}}_i$, the third corresponds to $\tilde{\tilde{u}}_3=\tilde{u}_3$, $\tilde{\tilde{u}}_1=\tilde{u}_1$, and the fourth corresponds to $\tilde{\tilde{u}}_3=-\tilde{u}_3$, $\tilde{\tilde{u}}_1=\tilde{u}_1$. The first two fixed points are attractive, the other two are saddle points. Which fixed point the system will flow to depends on the initial conditions. In our case all interactions are positive (repulsive), i.e., at the bare level $\tilde{u}_i$ are all positive and $\tilde{u}_i > \tilde{\tilde{u}}_i$. For these initial conditions, we verified that the system is outside the base of attraction of the second fixed point as it can be reached only if bare w_i are negative (at this fixed point $\tilde{u}_i$ vanishes compared to $\tilde{\tilde{u}}_i$, i.e., w_i/u_i tends to -1).

At the first attractive fixed point $\tilde{\tilde{u}}_i$ vanishes compared to $\tilde{u}_i$, i.e., w_i/u_i tends to 1. This is consistent with our initial conditions. Near this fixed point, $\tilde{\tilde{u}}_3$ can be neglected compared to $\tilde{u}_3$ in the equations for $\dot{u}_4$ and $\dot{u}_6$, and the first five RG equations form a closed set

$$\dot{\tilde{u}}_1 = \tilde{u}_1^2 + \tilde{u}_3^2,$$

$$\dot{\tilde{u}}_2 = 2\tilde{u}_1\tilde{u}_2 - 2\tilde{u}_2^2,$$

$$\dot{\tilde{u}}_3 = 4\tilde{u}_1\tilde{u}_3 - 2\tilde{u}_2\tilde{u}_3 - 2\tilde{u}_3(u_4+u_6),$$

$$2\dot{u}_4 = -(2u_4)^2 - \tilde{u}_3^2,$$

$$2\dot{u}_6 = -(2u_6)^2 - \tilde{u}_3^2. \tag{35}$$

Within the same approximation

$$\Gamma^{\mathrm{SDW}} = \tilde{u}_1 + \tilde{u}_3,$$

$$\Gamma^{s\pm} = -2u_4 + \tilde{u}_3. \tag{36}$$

Comparing these equations with the ones we obtained for the two-pocket model, Eqs. (10) and (11), we see that they are equivalent, up to overall renormalizations of the couplings, if we identify $2u_6$ in Eq. (35) with u_5 in Eq. (11). There is minor difference between the $\Gamma^{s\pm}$ in the two cases [$2u_4$ in Eq. (36) vs u_4+u_5 in Eq. (10)], but it vanishes at the fixed point. Acordingly, the RG flow of the couplings and the vertices is the same as in the two-pocket model, namely, SDW vertex remains dominant for all L up to a fixed point, and SC vertex changes sign at some L, becomes attractive at larger L

and becomes equal to the SDW vertex at the fixed point if, indeed, the fixed point is reached within parquet RG. This similarity with a two-pocket model was first noted by Haule[60] and can be understood if we note that in the five-pocket case SC pairing is the same as in four-pocket model (with extra combinatoric factor of 2 compared to two-pocket case), but SDW pairing is now possible between the two sets of electron pockets (see Fig. 21), this adds the combinatoric factor of 2 also to the renormalization of the SDW vertex.

We now need to understand what is the basis of attraction for this fixed point. For this, we consider the two other fixed points for which $\tilde{\tilde{u}}_3=\tilde{u}_3$, $\tilde{\tilde{u}}_1=\tilde{u}_1$, or $\tilde{\tilde{u}}_3=-\tilde{u}_3$, $\tilde{\tilde{u}}_1=\tilde{u}_1$. We show that both are saddle points, and both are unstable when the bare u_i and w_i are all positive.

Consider, for example, the fixed point at $\tilde{\tilde{u}}_1=\tilde{u}_1$ and $\tilde{\tilde{u}}_3=\tilde{u}_3$. At this fixed point $u_4/\tilde{u}_1=-3$, $\tilde{u}_3/\tilde{u}_1=\sqrt{15}$, and $u_6=0$. Expanding in $\delta=\tilde{u}_1-\tilde{\tilde{u}}_1$ and $\epsilon=\tilde{u}_3-\tilde{\tilde{u}}_3$, we obtain the set of coupled linear differential equations

$$\dot{\delta}=2\tilde{u}_1(\delta+\sqrt{15}\epsilon),$$

$$\dot{\epsilon}=4\tilde{u}_1(\sqrt{15}\delta+4\epsilon) \tag{37}$$

together with $\dot{\tilde{u}}_1=\tilde{u}_1^2+\tilde{u}_3^2=16\tilde{u}_1^2$. The solution of the set is $\epsilon=\epsilon_0(\tilde{u}_1)^\gamma$, $\delta=\delta_0(\tilde{u}_1)^\gamma$. Substituting and solving for the set of two linear equations for ϵ_0 and δ_0, we obtain $\gamma_1=11/8$ and $\gamma_2=-1/4$. For ϵ and δ which correspond to $\gamma=\gamma_1$, the fixed point is unstable, for $\gamma=\gamma_2$, it is stable. A simple analysis shows that γ_1 is the solution when $\epsilon_0/\delta_0>0$ while γ_2 is the solution when $\epsilon_0/\delta_0<0$. In our case, the bare values of ϵ and δ are $2w_3$ and $2w_1$, respectively, both are positive. Hence this fixed point is unstable, and the RG flow bring the system toward the stable fixed point at which $\tilde{\tilde{u}}_1$ and $\tilde{\tilde{u}}_3$ are both small. The stability analysis of the fixed point at $\tilde{\tilde{u}}_1=\tilde{u}_1$, or $\tilde{\tilde{u}}_3=-\tilde{u}_3$ yields the same results, leaving the fixed point with $\tilde{\tilde{u}}_i\ll\tilde{u}_i$ as the only stable fixed point.

We next consider how the results are modified due to angular dependence of the vertices. We found two effects. First, one of SC vertices Γ_1^{SC} can become attractive already at small L in the same way as in the three-pocket model studies in the previous section. Namely, the system adjusts $\cos 2\phi$ and angle-independent components of the gaps along the two electron FSs to minimize the effect of intrapocket Coulomb repulsion. Just as for three-pocket model, Γ_1^{SC} is attractive and scales as α^2 if we only include angular dependence of the pair-hopping u_3 and w_3 terms. Second, SC and SDW vertices do not become identical at the fixed point if α is nonzero. If we only include angular dependence of u_3, w_3 and u_1 and w_1 (and set them equal), we find that SC vertex becomes larger than SDW vertex very near fixed point. However, the effect is numerically very weak, even when $\alpha\sim 1$. In Fig. 22 we show the flow of SC and SDW vertices for $\alpha=0.3$. SC vertex eventually becomes larger, but this is truly weak effect.

The flow of SDW and SC vertices toward almost the same value in the five-pocket model has been found numerically by Thomale *et al.* within fRG study.[27] Our analytical RG results for this case again agree with their fRG, what, in our opinion, is another confirmation that the "topology" of the RG flow is chiefly determined by combinatoric effects.

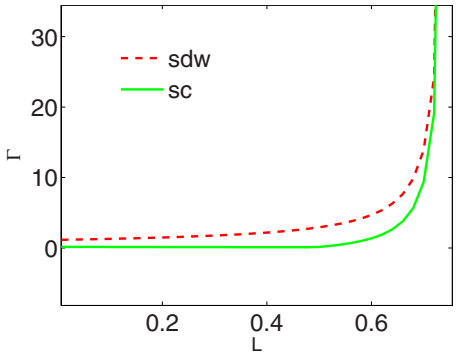

FIG. 22. (Color online) Parquet RG flow of SC and SDW vertices for the five-pocket model at $\alpha=0.3$. The SDW vertex remains the largest over the whole flow, and the ratio of the SDW and SC vertices approaches one at the fixed point of parquet RG. This is very similar to the two-pocket case except that here Γ^{SC} is attractive for all L.

3. RG flow below the scale of E_F

The system behavior for the case when the fixed point of the functional RG is not reached at $E>E_F$ is quite similar to the two-pocket model with the only difference that now SC instability always occurs when SDW order is destroyed by doping. Namely, at perfect nesting the system develops SDW order. At finite doping, the RG flow of the SDW vertex levels off, and SC vertex eventually becomes larger. The SC gap has $s\pm$ structure either without or with nodes along the electron FS, depending on the values of α and of $\log \Lambda/E_F$. The phase diagram is similar to that in Fig. 17 but only has the "SDW" region in that figure.

B. Five-pocket model with two equivalent hole FS at (0,0)

We now consider the opposite limit of five-pocket model when the two hole pockets centered at (0,0) are equivalent. Our goal is to verify whether the system behavior remains the same as in the limit when we keep only one of these two hole pockets.

The computations in the case of two equivalent hole pockets at (0,0) are quite involved and we only present the results for $\alpha=0$. Because the pockets at (0,0) and (π,π) are now non-equivalent [in the sense that there are two pockets at (0,0) and only one at (π,π)], the interactions involving these pockets do not need to flow to the same value under RG, e.g., u_i and w_i need not to fly to the same value, and also electron-hole and hole-hole interactions involving fermions from near (0,0) and (π,π) need not to be the same. Finally, SC gaps on the hole FSs at (0,0) and (π,π) also do not have to be equal.

1. Vertices

Keeping all this in mind and applying the same analysis as before we obtain the equations for the SDW and SC vertices. For the SDW, we introduce two vertices Δ_1 and Δ_2,

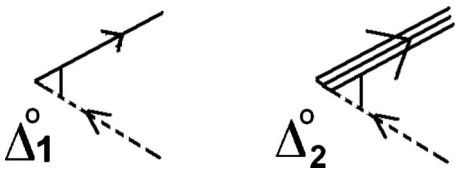

FIG. 23. The two nonequivalent SDW vertices in the five-pocket model with two identical hole FSs at (0,0). The triple solid line stands for the fermion (hole) at (π,π). These two vertices are present also for the case when there is only one hole FSs at (0,0), but in that case we set $\Delta_1^o=\Delta_2^o$ and verified that the equivalence also holds for renormalized $\Delta_{1,2}$.

shown in Fig. 23 and write the set of 2×2 coupled equations as

$$\begin{pmatrix} 1+2(u_1+u_3)L & (w_1+w_3)L \\ 2(w_1+w_3)L & 1+(\bar{u}_1+\bar{u}_3)L \end{pmatrix}\begin{pmatrix} \Delta_1^o \\ \Delta_2^o \end{pmatrix}=\begin{pmatrix} \Delta_1 \\ \Delta_2 \end{pmatrix}, \quad (38)$$

where the vertices $\bar{u}_1$ and $\bar{u}_3$ are shown in Fig. 24

For the SC vertex we introduce, as before, Δ_e, $\Delta_{h1}=\Delta[k=(0,0)]$ and $\Delta_{h2}=\Delta[k=(\pi,\pi)]$ and obtain

$$\begin{pmatrix} 1-2u_4L & -4u_3L & -\bar{u}_3L \\ -2u_3L & 1-4u_5L & -\bar{u}_5L \\ -2\bar{u}_3L & -4\bar{u}_5L & 1-\bar{\bar{u}}_5L \end{pmatrix}\begin{pmatrix} \Delta_e^o \\ \Delta_{h_1}^o \\ \Delta_{h_2}^o \end{pmatrix}=\begin{pmatrix} \Delta_e \\ \Delta_{h_1} \\ \Delta_{h_2} \end{pmatrix}. \quad (39)$$

The vertices $\bar{u}_5$ and $\bar{\bar{u}}_5$ are shown in Fig. 24.

2. Parquet RG equations

The total number of RG equations is quite large and we refrain from writing all of them. Quite predictably, the combinatoric factors associated with the existence of the two equivalent pockets at (0,0) give rise to relations $\bar{u}_i=2u_i$ $(i=1,3,5)$, $u_4=4u_5$, and $\bar{\bar{u}}_5=4u_5$. Using these relations, we obtain for the relevant couplings u_1,w_1,u_3,w_3 and u_4 the set

$$\dot{u}_1=2(u_1^2+u_3^2)+w_1^2+w_3^2,$$

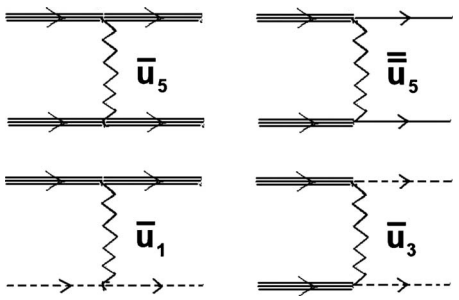

FIG. 24. The interactions involving fermions near the hole FS at (π,π) (the triple solid line). The dashed line stands for a fermion from an electronic pocket. For the case of only one hole FSs at (0,0) we set $\bar{u}_5=\bar{\bar{u}}_5=u_5$, $\bar{u}_1=u_1$, and $\bar{u}_3=u_3$ from the beginning and verified that these relations hold for running couplings. For the case of two identical hole pockets at (0,0), the fixed point values of the couplings involving fermions near (π,π) are different from those involving fermions near (0,0).

$$\dot{w}_1=4w_1u_1+4w_3u_3,$$

$$\dot{u}_3=4(2u_1u_3+w_1w_3)-4u_3u_4,$$

$$\dot{w}_3=8(u_1w_3+u_3w_1)-4u_6w_3,$$

$$2\dot{u}_4=-(2u_4)^2-16u_3^2,$$

$$2\dot{u}_6=-(2u_6)^2-8w_3^2. \quad (40)$$

Introducing now $\tilde{u}_1=2u_1+\sqrt{2}w_1, \tilde{\bar{u}}_1=2u_1-\sqrt{2}w_1$, $\tilde{u}_3=2u_3+\sqrt{2}w_3, \tilde{\bar{u}}_3=2u_3-\sqrt{2}w_3$ and substituting into Eq. (40) we obtain

$$\dot{\tilde{u}}_1=\tilde{u}_1^2+\tilde{u}_3^2,$$

$$\dot{\tilde{u}}_3=4\tilde{u}_1\tilde{u}_3-2\tilde{u}_3(u_4+u_6)-2\tilde{\bar{u}}_3(u_4-u_6),$$

$$2\dot{u}_4=-(2u_4)^2-(\tilde{u}_3+\tilde{\bar{u}}_3)^2,$$

$$2\dot{u}_6=-(2u_6)^2-(\tilde{u}_3-\tilde{\bar{u}}_3)^2,$$

$$\dot{\tilde{\bar{u}}}_1=\tilde{\bar{u}}_1^2+\tilde{\bar{u}}_3^2,$$

$$\dot{\tilde{\bar{u}}}_3=4\tilde{\bar{u}}_1\tilde{\bar{u}}_3-2\tilde{\bar{u}}_3(u_4+u_6)-2\tilde{u}_3(u_4-u_6). \quad (41)$$

This is exactly the same set as Eq. (34) that we obtained in the previous section (we skip the equation on u_2 which is irrelevant coupling anyway).

Under the same conditions $[\bar{u}_i=2u_i$ $(i=1,3,5)$, $u_4=4u_5$, and $\bar{\bar{u}}_5=4u_5]$, the relevant SDW and SC vertices become

$$\Gamma^{\mathrm{SDW}}=\tilde{u}_1+\tilde{u}_3,$$

$$\Gamma^{s\pm}=-2u_4+\tilde{u}_3+\tilde{\bar{u}}_3. \quad (42)$$

These again are the same equations as Eq. (33) for the case of only one hole FS at (0,0). The only difference with the other limit is that now the solutions corresponding to Γ^{SDW} and $\Gamma^{s\pm}$ from Eq. (42) are $\Delta_2=\sqrt{2}\Delta_1$ and $\Delta_{h2}=2\Delta_{h1}=-\Delta_e$.

We see therefore that the system behavior in the two limits is identical. Like in the four-pocket case, this equivalence strongly suggests that the same behavior holds also in the intermediate, most generic five-pocket model, when the two hole pockets at (0,0) are both present but are not identical.

C. Summary of the results for five-pocket model

We see that the system behavior in a five-pocket model is "intermediate" between two-pocket and four-pocket models. On one hand, like in a four-pocket model, the largest SC vertex can be positive already at the smallest L, even when intrapocket Coulomb repulsion is the dominant interaction. If this is the case, then there is no critical L before which SC vertex is repulsive, and the system always becomes a SC when the competing SDW instability is reduced. The SC gap is either nodeless or with nodes on electron FSs, depending

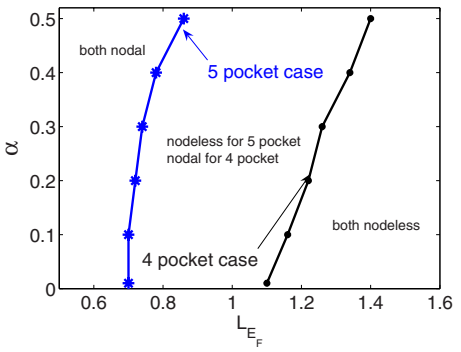

FIG. 25. (Color online) Comparison of the SC phases for four- and five-pocket models. The initial conditions are identical for the common parameters. The figure shows that there exists a parameter range where the SC gap is nodeless in the five-pocket model but is nodal in the four-pocket model.

on α, much like in the unshaded region in Fig. 14. On the other hand, like in a two-pocket model, SDW vertex remains larger than SC vertex for all L before the fixed point is reached, and the two vertices flow to the same value at the fixed point of parquet RG (Fig. 22). This last statement is exact when $\alpha=0$ and remains numerically quite accurate even when $\alpha \neq 0$ although strictly speaking, at a finite α, SC vertex eventually becomes larger than SDW vertex in the immediate vicinity of the fixed point.

D. Comparison of four-pocket and five-pocket models

It is instructive to compare the structures of the SC gaps in five-pocket and four-pocket models for the same values of input parameters (and using the same relations as above for extra parameters of a five-pocket model). This comparison is shown in Fig. 25. We see that there is quite wide parameter range where in the four-pocket model the gap has nodes while in the five-pocket model it is still nodeless. Each point in the phase diagram in Fig. 25 corresponds to some values of the couplings, hence this result implies that for a certain range of input parameters four-pocket model yields a gap with nodes while five-pocket model yields the gap without nodes. This agrees with the number of RPA studies[20,29,61] which found nodal gap for five-pocket model and no-nodal gap for four-pocket model. At the same time, our results show that in both models there are regions of parameters in which the SC gap is either no-nodal or has nodes.

VI. CONCLUSION

We have done calculations addressing on the same footing the issues of the interplay between intrapocket and interpocket Coulomb repulsion in the Fe-based superconductors, the competition between SC and SDW orders, and the angular dependence of the SC gap. We considered two-, four-, and five-pocket models for the pnictides and for each model considered the flow of the couplings and of SDW and SC vertices within analytical parquet RG scheme. We found that in all models, fluctuations in the SDW and SC channels are coupled at intermediate energies $\Lambda > E > E_F$ between the bandwidth and the Fermi energy, but decouple at energies below E_F. The system behavior below E_F is governed by conventional ladder RG, and each vertex flows according to $d\Gamma_i/dL=\Gamma_i^2$.

For the toy two-pocket model, earlier results showed[22,50] that SDW instability is the dominant one at perfect nesting. The SC vertex is repulsive at large energies but changes sign under parquet RG and become attractive above some RG scale. The SDW and SC couplings flow to the same value at the fixed point of RG equations, and the fixed point of parquet RG has extended $O(6)$ symmetry.[51] If the scale of E_F is reached before this fixed point, SDW order prevails at zero doping but is reduced and eventually destroyed at finite doping. Whether or not SC appears in place of SDW order depends on whether SC vertex already changes sign and becomes attractive at E_F. If superconductivity appears, the SC gap has a simple plus-minus structure.

The main goal of this paper was to understand how this scenario is modified in realistic four-pocket and five-pocket models. We considered both models in the two limits: one when one of the two hole pockets centered at (0,0) is weakly coupled to other pockets and can be neglected, and the other when the two hole pockets centered at (0,0) are equivalent. We found identical results in both limit what gives us confidence that the system behavior in the intermediate case of two nonequivalent hole pockets at (0,0) remains the same as in the two limits.

Our main results are the following: (1) in both four-pocket and five-pocket models electron-hole and electron-electron interactions are generally angle dependent. The most relevant angle dependence is in the form $\cos 2\phi$, where ϕ is the angle along an electron FS. Because of this angular dependence, there are three different vertices in the SC channel. One of these vertices turns out to be attractive, in most cases, beginning from the largest energies. The symmetry of the attractive interaction is extended $s\pm$ wave (as opposed to a conventional $s{+}{+}$). Other two SC vertices are repulsive at all scales.

(2) This attractive SC vertex favors the $s\pm$ state in which the gaps along hole FSs are angle-independent (up to $\cos 4\phi$ corrections), while the gaps along the two electron FSs are in the form $\Delta_e \pm \bar{\Delta}_e \cos 2\phi$. The interplay between Δ_e and $\bar{\Delta}_e$ depends on the strength of $\cos 2\phi$ component of the interaction and also on the interplay between intrapocket and interpocket Coulomb repulsions. Depending on the parameters, the electron gaps can be either nodeless ($\Delta_e > \bar{\Delta}_e$), or have accidental nodes ($\Delta_e < \bar{\Delta}_e$).

(3) In five-pocket model at perfect nesting, the SDW vertex remains larger than this attractive SC vertex. The two flow up to the same values at the fixed point, if this fixed point is at an energy larger than E_F, and the fixed point has enlarged symmetry. This behavior is exact when the vertices are angle independent but only very weakly changes due to angular dependence of the vertices. If the system flows down to E_F without yet reaching the fixed point, SDW order wins. Away from perfect nesting SDW order is suppressed, and the system eventually develops a SC instability.

(4) In four-pocket model, the situation is similar at large E (i.e., at small RG parameter $\log \Lambda/E$) but before the fixed

point of parquet RG is reached, SC vertex becomes larger than SDW vertex. If this happens before the scale of E_F is reached, the system develops SC instability already at perfect nesting, and SDW instability does not appear. If SDW vertex remains the largest down to E_F, the system develops SDW instability at and around perfect nesting, and SC instability at larger dopings.

(5) We found that the SC gap is more likely to have accidental nodes on electron FSs in four-pocket model than in five-pocket model. Namely, for the same input parameters, there is a parameter range where the gap is nodal in four-pocket model and no-nodal in five-pocket model. This agrees with several RPA-type studies based on spin fluctuations.[20,29,61] Still, we found that in both four-pocket and five-pocket model the gap can be either nodal or nodeless, depending on parameters.

Our analytical results are fully consistent with numerical fRG study of four-pocket and five-pocket models by Thomale *et al.*[27] We view this agreement as the evidence that the differences between four-pocket and five-pocket models are geometrical (different combinatorics in RG equations), and are captured already within analytical one-loop RG. We note in this regard that we found that the difference between four-pocket and five-pocket models is not caused by the angular dependence of the interaction and holds even when interactions are angle independent.

The results for the four-pocket case demonstrate that SDW order need not be pre-requisite to SC± order, although for most part of the phase diagram it does appear at perfect nesting, and SC only appears upon doping. We also emphasize that the interplay between SC and SDW is both "mutual support" and "competition." Namely, SC and SDW *fluctuations* tend to enhance each other, what is relevant is the fact that in the applicability range of parquet RG (when SC and SDW fluctuations talk to each other), both SC and SDW vertices diverge upon approaching the fixed point. At the same time, SDW and SC *orders* compete with each other,[58,59] meaning that SC order only emerges when SDW order is reduced enough by doping, and SDW order does not emerge at all if SC order emerges first already at perfect nesting.

ACKNOWLEDGMENTS

We acknowledge helpful discussions with L. Benfatto, R. Fernandes, W. Hanke, P. Hirschfeld, I. Eremin, Y. Matsuda, I. Mazin, R. Prozorov, D. Scalapino, J. Schmalian, Z. Tesanovic, R. Thomale, M. Vavilov, and A. Vorontsov. We also thank I. Mazin for careful reading of the MS and useful comments. This work was supported by NSF-DMR-0906953. Partial support from MPI PKS (Dresden) (S.M. and A.V.C), Ruhr-Univerisity Bochum (S.M), and Humboldt foundation (A.V.C) is gratefully acknowledged.

[1] For recent reviews see D. C. Johnston, Adv. Phys. **59**, 803 (2010); J.-P. Paglione and R. L. Greene, Nat. Phys. **6**, 645 (2010).

[2] Y. Kamihara, T. Watanabe, M. Hirano, and H. Hosono, J. Am. Chem. Soc. **130**, 3296 (2008).

[3] X. H. Chen, T. Wu, G. Wu, R. H. Liu, H. Chen, and D. F. Fang, Nature (London) **453**, 761 (2008).

[4] G. F. Chen, Z. Li, D. Wu, G. Li, W. Z. Hu, J. Dong, P. Zheng, J. L. Luo, and N. L. Wang, Phys. Rev. Lett. **100**, 247002 (2008).

[5] Z.-A. Ren, G.-C. Che, X.-L. Dong, J. Yang, W. Lu, W. Yi, X.-L. Shen, Z.-C. Li, L.-L. Sun, F. Zhou, and Z.-X. Zhao, EPL **83**, 17002 (2008).

[6] M. Rotter, M. Tegel, and D. Johrendt, Phys. Rev. Lett. **101**, 107006 (2008).

[7] K. Sasmal, B. Lv, B. Lorenz, A. M. Guloy, F. Chen, Y.-Y. Xue, and C.-W. Chu, Phys. Rev. Lett. **101**, 107007 (2008).

[8] N. Ni, A. Thaler, J. Q. Yan, A. Kracher, E. Colombier, S. L. Bud'ko, P. C. Canfield, and S. T. Hannahs, Phys. Rev. B **82**, 024519 (2010).

[9] X. Wang, Q. Liu, Y. Lv, W. Gao, L. Yang, R. Yu, F. Li, and C. Jin, arXiv:0806.4688 (unpublished); S. V. Borisenko, V. B. Zabolotnyy, D. V. Evtushinsky, T. K. Kim, I. V. Morozov, A. N. Yaresko, A. A. Kordyuk, G. Behr, A. Vasiliev, R. Follath, and B. Büchner, Phys. Rev. Lett. **105**, 067002 (2010).

[10] Y. Mizuguchi, F. Tomioka, S. Tsuda, T. Yamaguchi, and Y. Takano, Appl. Phys. Lett. **93**, 152505 (2008); F. C. Hsu, J.-Y. Luo, K.-W. Yeh, T.-K. Chen, T.-W. Huang, P. M. Wu, Y.-C. Lee, Y.-L. Huang, Y.-Y. Chu, D.-C. Yan, and M.-K. Wu, Proc. Natl. Acad. Sci. U.S.A. **105**, 14262 (2008); M. H. Fang, H. M. Pham, B. Qian, T. J. Liu, E. K. Vehstedt, Y. Liu, L. Spinu, and Z. Q. Mao, Phys. Rev. B **78**, 224503 (2008); G. F. Chen, Z. G. Chen, J. Dong, W. Z. Hu, G. Li, X. D. Zhang, P. Zheng, J. L. Luo, and N. L. Wang, *ibid.* **79**, 140509(R) (2009); B. Zeng, G. Mu, H. Luo, T. Xiang, H. Yang, L. Shan, C. Ren, I. Mazin, P. Dai, and H. Wen, arXiv:1007.3597 (unpublished).

[11] C. de la Cruz, Q. Huang, J. W. Lynn, J. Li, W. Ratcliff II, J. L. Zarestky, H. A. Mook, G. F. Chen, J. L. Luo, N. L. Wang, and P. Dai, Nature (London) **453**, 899 (2008); for the latest results on magnetic measaurements, see D. S. Inosov, J. T. Park, P. Bourges, D. L. Sun, Y. Sidis, A. Schneidewind, K. Hradil, D. Haug, C. T. Lin, B. Keimer, and V. Hinkov, Nat. Phys. **6**, 178 (2010), and references therein.

[12] Y. Kamihara, H. Hiramatsu, M. Hirano, R. Kawamura, H. Yanagi, T. Kamiya, and H. Hosono, J. Am. Chem. Soc. **128**, 10012 (2006).

[13] M. Yi, D. H. Lu, J. G. Analytis, J.-H. Chu, S.-K. Mo, R.-H. He, R. G. Moore, X. J. Zhou, G. F. Chen, J. L. Luo, N. L. Wang, Z. Hussain, D. J. Singh, I. R. Fisher, and Z.-X. Shen, Phys. Rev. B **80**, 024515 (2009).

[14] S. E. Sebastian, J. Gillett, N. Harrison, P. H. C. Lau, D. J. Singh, C. H. Mielke, and G. G. Lonzarich, J. Phys.: Condens. Matter **20**, 422203 (2008).

[15] D. J. Singh and M.-H. Du, Phys. Rev. Lett. **100**, 237003 (2008); M. J. Calderón, B. Valenzuela, and E. Bascones, Phys. Rev. B **80**, 094531 (2009).

[16] L. Boeri, O. V. Dolgov, and A. A. Golubov, Phys. Rev. Lett.

101, 026403 (2008).
[17] I. I. Mazin, D. J. Singh, M. D. Johannes, and M. H. Du, Phys. Rev. Lett. **101**, 057003 (2008).
[18] S. Onari and H. Kontani, arXiv:1009.3882 (unpublished).
[19] K. Kuroki, S. Onari, R. Arita, H. Usui, Y. Tanaka, H. Kontani, and H. Aoki, Phys. Rev. Lett. **101**, 087004 (2008).
[20] K. Kuroki, H. Usui, S. Onari, R. Arita, and H. Aoki, Phys. Rev. B **79**, 224511 (2009).
[21] K. Seo, B. A. Bernevig, and J. Hu, Phys. Rev. Lett. **101**, 206404 (2008).
[22] A. V. Chubukov, D. V. Efremov, and I. Eremin, Phys. Rev. B **78**, 134512 (2008).
[23] V. Stanev, J. Kang, and Z. Tesanovic, Phys. Rev. B **78**, 184509 (2008); V. Stanev, B. Alexandrov, P. Nokolić, and Z. Tešanović, arXiv:1006.0447 (unpublished).
[24] S. Graser, T. A. Maier, P. J. Hirshfeld, and D. J. Scalapino, New J. Phys. **11**, 025016 (2009).
[25] Fa Wang, H. Zhai, Y. Ran, A. Vishwanath, and D.-H. Lee, Phys. Rev. Lett. **102**, 047005 (2009).
[26] C. Platt, C. Honerkamp, and W. Hanke, New J. Phys. **11**, 055058 (2009); R. Thomale, C. Platt, J. Hu, C. Honerkamp, and B. A. Bernevig, Phys. Rev. B **80**, 180505 (2009).
[27] R. Thomale, C. Platt, W. Hanke, and B. Bernevig, arXiv:1002.3599 (unpublished).
[28] A. V. Chubukov, M. G. Vavilov, and A. B. Vorontsov, Phys. Rev. B **80**, 140515(R)(2009).
[29] A. F. Kemper, T. A. Maier, S. Graser, H.-P. Cheng, P. J. Hirschfeld, and D. J. Scalapino, New J. Phys. **12**, 073030 (2010).
[30] Y. Nakai, K. Ishida, Y. Kamihara, M. Hirano, and H. Hosono, J. Phys. Soc. Jpn. **77**, 073701 (2008).
[31] H.-J. Grafe, D. Paar, G. Lang, N. J. Curro, G. Behr, J. Werner, J. Hamann-Borrero, C. Hess, N. Leps, R. Klingeler, and B. Büchner, Phys. Rev. Lett. **101**, 047003 (2008).
[32] Y. Wang, L. Shan, L. Fang, P. Cheng, C. Ren, and H.-H. Wen, Supercond. Sci. Technol. **22**, 015018 (2009).
[33] O. Millo, I. Asulin, O. Yuli, I. Felner, Z.-A. Ren, X.-L. Shen, G.-C. Che, and Z.-X. Zhao, Phys. Rev. B **78**, 092505 (2008).
[34] J. D. Fletcher, A. Serafin, L. Malone, J. G. Analytis, J.-H. Chu, A. S. Erickson, I. R. Fisher, and A. Carrington, Phys. Rev. Lett. **102**, 147001 (2009).
[35] C. W. Hicks, T. M. Lippman, M. E. Huber, J. G. Analytis, J.-H. Chu, A. S. Erickson, I. R. Fisher, and K. A. Moler, Phys. Rev. Lett. **103**, 127003 (2009).
[36] K. Hashimoto *et al.*, Phys. Rev. B **81**, 220501(R) (2010).
[37] J.-Ph. Reid, M. A. Tanatar, X. G. Luo, H. Shakeripour, N. Doiron-Leyraud, N. Ni, S. L. Bud'ko, P. C. Canfield, R. Prozorov, and L. Taillefer, Phys. Rev. B **82**, 064501 (2010).
[38] Y. Nakai, T. Iye, S. Kitagawa, K. Ishida, H. Ikeda, S. Kasahara, H. Shishido, T. Shibauchi, Y. Matsuda, and T. Terashima, Phys. Rev. Lett. **105**, 107003 (2010).
[39] R. T. Gordon, H. Kim, N. Salovich, R. W. Giannetta, R. M. Fernandes, V. G. Kogan, T. Prozorov, S. L. Bud'ko, P. C. Canfield, M. A. Tanatar, and R. Prozorov, Phys. Rev. B **82**, 054507 (2010).
[40] K. Hashimoto, A. Serafin, S. Tonegawa, R. Katsumata, R. Okazaki, T. Saito, H. Fukazawa, Y. Kohori, K. Kihou, C. H. Lee, A. Iyo, H. Eisaki, H. Ikeda, Y. Matsuda, A. Carrington, and T. Shibauchi, Phys. Rev. B **82**, 014526 (2010).
[41] K. Hashimoto, T. Shibauchi, T. Kato, K. Ikada, R. Okazaki, H. Shishido, M. Ishikado, H. Kito, A. Iyo, H. Eisaki, S. Shamoto, and Y. Matsuda, Phys. Rev. Lett. **102**, 017002 (2009).
[42] L. Malone, J. D. Fletcher, A. Serafin, A. Carrington, N. D. Zhigadlo, Z. Bukowski, S. Katrych, and J. Karpinski, Phys. Rev. B **79**, 140501(R) (2009).
[43] K. Nakayama, T. Sato, P. Richard, Y. Xu, T. Kawahara, K. Umezawa, T. Qian, M. Neupane, G. Chen, H. Ding, and T. Takahashi, arXiv:1009.4236 (unpublished), and references therein.
[44] D. S. Inosov, J. S. White, D. V. Evtushinsky, I. V. Morozov, A. Cameron, U. Stockert, V. B. Zabolotnyy, T. K. Kim, A. A. Kordyuk, S. V. Borisenko, E. M. Forgan, R. Klingeler, J. T. Park, S. Wurmehl, A. N. Vasiliev, G. Behr, C. D. Dewhurst, and V. Hinkov, Phys. Rev. Lett. **104**, 187001 (2010).
[45] C. Liu, A. Palczewski, T. Kondo, R. Fernandes, E. Mun, H. Hodovanets, A. N. Thaler, J. Schmalian, S. Bud'ko, P. Canfield, and A. Kaminski, arXiv:1011.0980 (unpublished), and references therein.
[46] Z. Liu, P. Richard, K. Nakayama, G. Chen, S. Dong, J. He, D. Wang, T. Xia, K. Umezawa, T. Kawahara, S. Souma, T. Sato, T. Takahashi, T. Qian, Y. Huang, N. Xu, Y. Shi, H. Ding, and S. Wang, arXiv:1008.3265 (unpublished).
[47] S. Onari and H. Kontani, Phys. Rev. Lett. **103**, 177001 (2009).
[48] W. L. McMillan, Phys. Rev. **167**, 331 (1968); N. N. Bogolubov, V. V. Tolmachev, and D. V. Shirkov, Consultants Bureau, 1959.
[49] I. Mazin and J. Schmalian, Physica C **469**, 614 (2009).
[50] A. V. Chubukov, Physica C **469**, 640 (2009).
[51] D. Podolsky, H.-Y. Kee, and Y. B. Kim, EPL **88**, 17004 (2009).
[52] D. J. Singh, Phys. Rev. B **78**, 094511 (2008).
[53] I. Aleiner, B. L. Altshuler, and A. V. Chubukov (unpublished).
[54] J. F. Annett, N. Goldenfeld, and A. J. Leggett, J. Low Temp. Phys. **105**, 473 (1996).
[55] P. Monthoux and D. Pines, Phys. Rev. B **49**, 4261 (1994); D. J. Scalapino, Phys. Rep. **250**, 329 (1995); Ar. Abanov, A. V. Chubukov, and M. R. Norman, Phys. Rev. B **78**, 220507 (2008).
[56] S. Maiti, M. M. Korshunov, T. A. Maier, and A. V. Chubukov (unpublished).
[57] I. Eremin and A. V. Chubukov, Phys. Rev. B **81**, 024511 (2010).
[58] R. M. Fernandes and J. Schmalian, Phys. Rev. B **82**, 014521 (2010).
[59] A. B. Vorontsov, M. G. Vavilov, and A. V. Chubukov, Phys. Rev. B **81**, 174538 (2010); M. G. Vavilov, A. V. Chubukov, and A. B. Vorontsov, Supercond. Sci. Technol. **23**, 054011 (2010).
[60] K. Haule (unpublished).
[61] S. Graser, A. F. Kemper, T. A. Maier, H.-P. Cheng, P. J. Hirschfeld, and D. J. Scalapino, Phys. Rev. B **81**, 214503 (2010).